

Folding with a protein's native shortcut network

Susan Khor
slc.khor@gmail.com
(Oct 31, 2016)

Abstract

The physical basis of shortcut edges in a Protein Residue Network (PRN) and their applicability to a simplified protein folding pathway problem is investigated. The results show promise, and suggest the dominant influence of native-state topology even for structurally homologous proteins with different preferred folding pathways. Shortcut edges are enriched with hydrogen bonds, and there is a significant strong negative correlation (Pearson's rho -0.7591) between their relative contact order and the folding rates of 44 small and structurally diverse proteins. The initial folding reaction points identified for several single-domain proteins including LB1, GB1, and GB1's two variants NuG1 and NuG2, by the clustering coefficient computed on the ShortCut Network (SCN), are in agreement with experimental and theoretical evidence. Also observed, but with PRNs, is that key folding sites have more rigid profiles.

1. Introduction

The problem of knowing how a biological sequence of amino acids finds its functional configuration from a denatured state in the crowded environment of a cell has been around for at least half a century [1]. The difficulty of this problem is compounded by the impossibility of an unbiased random search solution for the fast folding rates required [2]. And hence the existence of preferred or dominant protein folding pathways was conjectured, and the problem of what determines a protein's folding pathway(s) arose¹ [3].

An early and still influential response to this challenge is the native-state topology hypothesis which proposes that protein folding rates and mechanisms are largely determined by the native structures of proteins [6]. A strong evidence for this hypothesis is the significant negative correlation between the folding rates of small proteins and their relative contact order (RCO), which is a simple complexity measure of a protein's native topology [7, 8].

An implication of this hypothesis is that structurally homologous proteins fold in similar ways and therefore are expected to exhibit similar folding pathways. However, the discovery of two structurally homologous, nearly symmetric proteins (proteins G and L) that fold differently, but with folding rates that are within one order of magnitude from each other [9] motivated a re-visit of and search for other determinants of protein folding pathways. Structurally homologous proteins with little sequence identity (e.g. proteins G and L have only 15% sequence identity in a structure-based alignment [9]) also throw a wrench into the similar sequences produce similar folds hypothesis, which is a foundational principal of database approaches to protein structure prediction. Hence, despite the success of the database approaches to protein structure prediction, we still need to know the principles behind *ab-initio* protein folding, and proteins in edge cases form informative case studies to solve the protein sequence-structure puzzle [10, 11].

In this paper, we use a restricted binary collision (RBC) model (section 2.4) to explore the applicability of the clustering coefficient of a protein's native shortcut network (C_{SCN0}) (section 2.2) to identify plausible protein folding pathways. The concept of a shortcut edge was introduced previously in [12]. Section 2.1 describes the process of identifying shortcuts from a Protein Residue Network (PRN).

Our RBC model borrows heavily from Yang and Sze's mesoscopic approach [13], which follows in the tradition of studies that take a low-resolution approach to protein folding and rely only on native interactions (Gō models) to navigate the energy landscape of protein configurations [14]. However, our model restricts the configuration search space somewhat, and instead of an energy function we use the structural metric C_{SCN0} to bias the search. This change in the search bias not only relieves our method of

¹ See also [4] and [5] for the "different" views of protein folding.

the complexity of energy calculations, but if successful, could help to tether the ShortCut Network (SCN) abstraction to the physical interactions that govern protein folding. Moreover, Anfinsen's thermodynamic hypothesis [15] is not universal for proteins² and a non-energetic search bias may be informative in new complementary ways to the thermodynamic view of protein folding.

2. Definitions, Materials and Method

2.1 Shortcut edges and the shortcut network (SCN)

Shortcut edges are found by the Euclidean-distance Directed Search (EDS) algorithm when constructing paths on a PRN. The construction of a PRN from a protein's coordinates file³ (obtained from the PDB [18] or a Molecular Dynamics (MD) simulation), the EDS algorithm and shortcut edges were introduced in [12]. A SCN is a subgraph of a PRN induced by its set of shortcut edges. We suffix SCN and PRN with '0' to denote that the respective graphs are derived from a native-state protein configuration.

PRN construction is based on the method in refs. [19] and [20], but we consider both main- and side-chain atoms when evaluating interaction strength between residues to form PRN edges. The limitations of main-chain only or side-chain only coarse-grained models of protein folding have been contemplated [21, 22]. Our mixed approach is not unique. For instance, Kolinski's CABS model [23, 24] uses $C\alpha$, $C\beta$, side group and peptide bond positional information with a knowledge-based statistical potential contextually dependent on secondary structure information. ProPHet uses two pseudo-atoms per residue (one for $C\alpha$ and another for side-chain atoms, except GLY), in its elastic-network representation of proteins [25]. We also note that ref. [19] included main-chain hydrogen bond information in their classifier to distinguish decoy from native conformations.

What is perhaps a little unusual for a protein folding model is peptide bonds are prohibited as PRN edges. This design choice was inherited from [19] (models that exclude other types of "obvious" edges exists as well) and has so far shown itself to be a fortuitous one. It has allowed investigation of allosteric communication in proteins [26], and provided this research is successful, it potentially equips the PRN model to facilitate an integrated investigation into protein folding and dynamics [27]. We note that peptide bond effects, i.e. distance fluctuations (or rather lack thereof) between residues adjacent on the protein sequence, are commonly excluded when examining native protein dynamics, e.g. COMMA [28] and the force constant calculation in ref. [25]. The inclusion of peptide bonds in PRNs has a detrimental effect on shortcut edges (Fig. A1). This suggests that the exclusion of peptide bonds is forcing EDS to find an alternative route, and in the process gather geometric information about the protein backbone.

EDS is a greedy local search algorithm similar to Kleinberg's [29] but with backtracking. Let $\mathcal{U}(p)$ be the union of the direct neighbors of all nodes in a path $p = \langle s \dots a \dots b \dots c \rangle$ where s is the source node and c is the most recent node appended to p . EDS adds a node z that is not already in p to p if z is closest (in Euclidean distance) to the target node amongst all nodes in $\mathcal{U}(p)$. Each time EDS adds a node not already in a path, the new node is given a *timestamp*. Let $T(v)$ be a positive integer denoting the timestamp of node v on an EDS path. Node timestamps start at 1 for the source (first) node in a path, and increase by one for each *new* node added to a path. If z is adjacent to c , then z is appended to p , i.e. $p = \langle s \dots a \dots b \dots c, z \rangle$. Otherwise, EDS backtracks to the node in p with the largest timestamp that is adjacent to z . If for instance, z is in the direct neighborhoods of both a and b , EDS backtracks to b to reach z since $T(b) > T(a)$, and $p = \langle s \dots a \dots b \dots c \dots b, z \rangle$. Fig. 1 demonstrates the construction of EDS paths and identification of shortcut edges. Fig.2 illustrates the shortcuts within the 1BDD protein.

An edge (u, v) is a *shortcut* if and only if $T(v) = T(u) + 1$, and v is adjacent to a node w such that $T(w) < T(u)$. Shortcut edges help EDS avoid backtracking. For instance, without the shortcut (57, 54) in Fig. 1-left, EDS needs to backtrack to node 55 and then to node 40 to reach node 54. The condition $T(v) = T(u) +$

² For example, the native structures of alpha-lytic protease [16] and serpins [17] do not correspond to the minimum free-energy basin.

³ The threshold for I_{uv} is incorrectly stated in [12] as ≥ 0.5 , this is corrected in [26] as ≥ 0.05 .

1 is necessary so that the process of backtracking itself does not create shortcut edges. For example, without this condition, (74, 77) in Fig. 1-center would be incorrectly identified as a shortcut edge for this path as a result of EDS backtracking from node 76 to reach node 77. Incidentally, (74, 77) is a shortcut in this PRN, but is identified as so by other EDS paths.

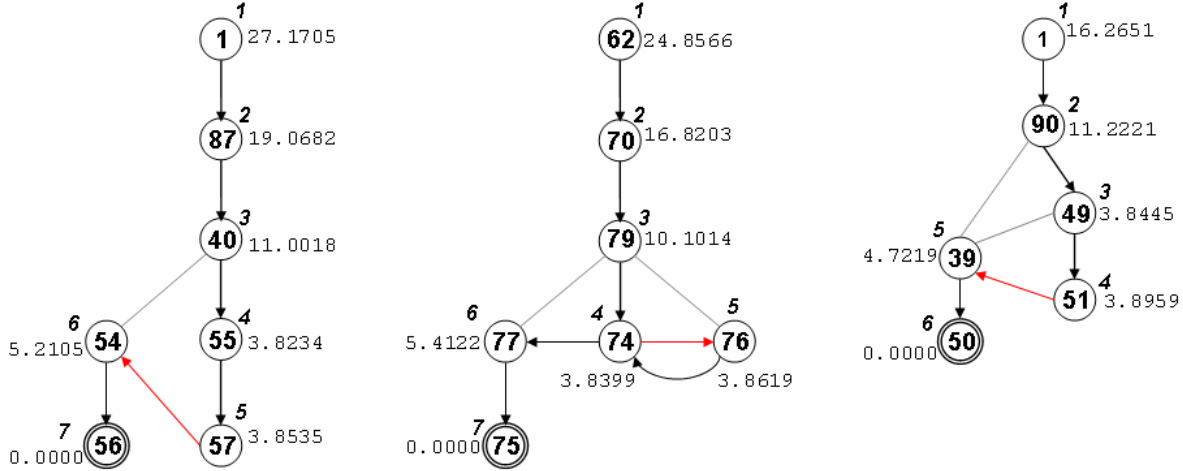


Fig. 1 Three EDS paths from 2EZN PRNs. PRN edges are undirected, but the edges are oriented in the diagram in the direction they are traversed by EDS in the respective paths. Un-oriented edges are not traversed, but exist and play a role in determining whether an edge is a shortcut. Shortcut edges are marked in red. The real number besides each node is the node's Euclidean distance to the target node. The italicized integer besides each node v is the node's timestamp or $T(v)$ value. The leftmost EDS path is of length six and is $\langle 1, 87, 40, 55, 57, 54, 56 \rangle$. It has one shortcut edge (57, 54). The center EDS path is of length seven and is $\langle 62, 70, 79, 74, 76, 74, 77, 75 \rangle$. It has one shortcut edge (74, 76). The rightmost EDS path is of length five and is $\langle 1, 90, 49, 51, 39, 50 \rangle$. It has one shortcut edge (51, 39).

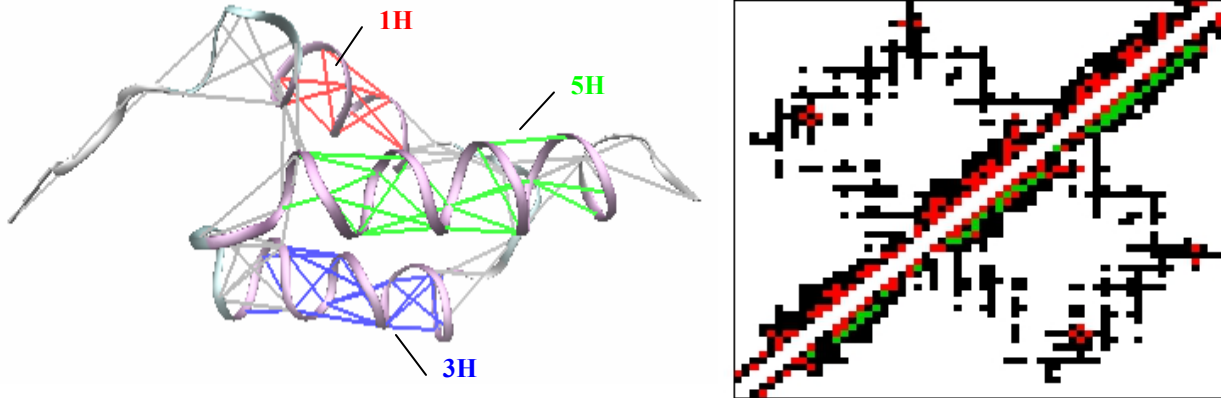


Fig. 2 Left: Shortcut edges are drawn on a cartoon of 1BDD with VMD [30]. Shortcuts within the three helix structures 1H, 3H and 5H are colored red, blue and green respectively. Right: Adjacency matrix (contact map) of 1BDD's PRN. Shortcut edges are marked by red cells, non-shortcut edges by black cells and (in the lower triangle only) hydrogen bonds identified with HBPLUS version 3.2 [31] that coincide with edges by green cells.

2.2 SCN clustering coefficient

The clustering coefficient C of a graph G is the average clustering coefficient over all its nodes N , i.e.

$$C_G = \frac{1}{N} \sum_i C(i). \text{ The clustering coefficient of a node is } C(i) = \frac{2e_i}{k_i(k_i - 1)}$$

where e is the number of links between node i 's k direct neighbors [32]. $C_{\text{SCN}} (C_{\text{PRN}})$ refers to a clustering coefficient computed using the

edges of a SCN (PRN) exclusively. We use C_{SCN0} and C_{PRN0} to indicate that the respective statistics are derived from a native-state configuration.

2.3 Protein dataset and its characteristics

The PDB coordinate files of the 18 proteins in this study (Table A1) were downloaded from rcsb.org [18], and a SCN0 was constructed for each. The PDB coordinates of both 1MHX and 1MI0 required side-chain reconstruction by DeepView [33], and the reconstructed 1MI0:A structure needed energy minimization for DeepView to produce an error-free energy report. Energy minimization is performed one cycle at a time using steepest descend with all residues selected.

The SCN0 characteristics of the 18 proteins (Table A3) concur with previous observations on a larger set of PRNs [12]. A native SCN spans almost all the nodes of its protein, $N_{\text{SCN0}} \approx N$. The ratio of the number of native shortcut edges to the number of nodes in a protein ($|\text{SC}|/N$) ranges from 1.43 to 1.99. One of the major differences between PRN0s and their SCN0s, besides the number of edges, is the type of edges. SCN0s are composed of significantly (one-sided paired t.test p-value < 0.01) more *short-range edges* (SE) than PRN0s. An edge is short-range if it connects residues that are at most 10 positions apart on a protein sequence, and long-range otherwise. Averaged over the 18 proteins, 51% of PRN0 edges and 68% of SCN0 edges are short-range. SCN0 edges are also significantly (one-sided paired t.test p-value < 0.01) shorter than PRN0 edges in terms of the maximum C α -C α Euclidean distance between their endpoints.

Of the 18 proteins, we chose seven structurally diverse (α , β and α/β) (Table A2) proteins which are archetypes of the protein folding pathway problem to test the applicability of our method. 2IGD (1GB1) and 2PTL are structural homologues with low (15%) sequence identity but with different folding pathways [9]. 2CI2 fold via the nucleation condensation mechanism wherein secondary and tertiary structures form simultaneously (stability of embryonic secondary structures need support from tertiary or long-range interactions) [34] and thus may prove challenging for our strict bottom-up hierarchical approach. Nevertheless, refs. [35, 36] argue that the nucleation condensation mechanism can be reconciled with the framework model, and Young and Sze [13] showed that a coarse-grained framework approach based on energetics can work for 2CI2.

2.4 Overview of our Restricted Binary Collision (RBC) model

In the RBC model, protein folding begins with an initial set of fully formed, isolated secondary structure elements (SSE) and terminates with the native conformation. In each fold step, exactly two secondary structure units (SSU) are collided to form an intermediate conformation, and this process is iterated until all the SSEs of a protein are combined into a conformation. Throughout this combining process, SSEs are assumed to be rigid fragments adopting their native structures. The challenge is to identify a sequence of intermediate conformations that can meaningfully, i.e. supported by simulation or experiment, form a folding pathway for a protein. Since one collision happens at each step, the process terminates in $n-1$ steps where n is the number of SSEs. The number of candidate conformations at each step reduces by one as the search approaches its target (native conformation). The total number of conformations (and thus the number of fitness function evaluations) involved in the search for a folding pathway is $n(n-1)/2$. The C_{SCN0} and the E folding pathways in section 3.3 were easily produced on an ordinary laptop PC running un-optimized Visual C++ code on Windows OS.

2.5 Secondary structure elements and (un)feasible secondary structure units

A *secondary structure element* (SSE) is a maximal contiguous segment of a protein sequence with the same secondary structure assignment, i.e. either H (helix), S (strand), or T (turn). The set of SSEs for each of the seven proteins examined are listed in Table A2. The SSEs of a protein are arranged in protein sequence order in a ring for the combining process in our RBC model (Fig. 3).

A *secondary structure unit* (SSU) comprises one or more non-Turn SSEs, and all Turn SSEs sandwiched between any of its non-Turn SSEs in the ring of SSEs. Table 1 enumerates all possible SSUs for 1BDD with their respective SSE constituents.

We consider a SSU *unfeasible* if it does not respect protein chain continuity. For instance, 1BDD's SSU (1H, 5H) is unfeasible because its SSE residues do not occupy a contiguous segment of the protein sequence. This restriction aligns with the principal that protein folding prefers paths that reduce the probability of premature conformational entropy loss [37, 38]. In essence, this principal prioritizes the formation of short-range before long-range edges. Notice that SSU (1H, 5H) is the only non-native SSU with long-range shortcuts (Table 1). Several protein folding models ensure that contact between a pair of residues is formed only when all intervening contacts are formed, or alternatively when all intervening residues are in their native positions [14, 39]. Thus our search space is confined to SSUs whose constituent SSEs can trace an uninterrupted path on the ring of SSEs without crossing the point where the N- and C- termini meet. We include unfeasible SSUs in our search diagrams (Appendix B) for completeness, and so that our folding pathways can be compared with those generated in [13] which does not enforce this restriction.

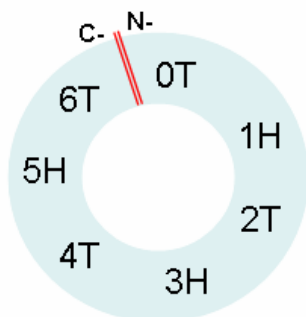


Fig. 3 Top: IBDD SSEs arranged in protein sequence order in a ring to construct SSUs.

Table 1 Secondary structure units (SSU) for 1BDD, their constituent SSEs and associated Conformation. Respectively, #, |SC|, |SCSE| and |SCLE| are the number of residues, shortcuts, shortcuts which are short-range and shortcuts which are long-range in a SSU.

SSU	SSEs in SSU	#	SC	SCSE	SCLE	Conformation
(1H)	1H	8	10	10	0	(1H) (3H) (5H)
(3H)	3H	13	21	21	0	(1H) (3H) (5H)
(5H)	5H	15	20	20	0	(1H) (3H) (5H)
(1H 3H)	1H, 2T, 3H	28	41	41	0	(1H, 3H) (5H)
(3H 5H)	3H, 4T, 5H	32	51	51	0	(3H, 5H) (1H)
(1H 5H)	0T, 1H, 5H, 6T	36	47	43	4	(1H, 5H) (3H)
(1H 3H 5H)	0T, 1H, 2T, 3H, 4T, 5H, 6T	60	90	84	6	(1H, 3H, 5H)

2.6 Conformations and their search space

A *Conformation* is a combination of one or more SSUs such that it contains all the non-Turn SSEs of a protein. Table 1 lists all of 1BDD's Conformations. Turn SSEs between SSUs are not added when forming Conformations. For example, 0T, 2T and 6T are excluded from Conformation (3H, 5H) (1H).

In general, a (discrete) search space is a graph G whose nodes represent unique combinations and whose edges represent permitted transformations between combinations. Similarly, in a Conformation search space graph, the nodes denote Conformations and the edges denote (kinetic) *accessibility* of one Conformation from another. A Conformation Y that can be derived from another Conformation X via a binary collision of X 's SSUs is accessible from X . For instance Conformation (1H 3H)(5H) is accessible from Conformation (1H)(3H)(5H) because it can be derived by combining (1H) and (3H). Fig. 4 depicts 1BDD's Conformation search space.

Implicit in our definition of Conformation accessibility is an impetus to construct Conformations with fewer SSUs, and the edges of our Conformation search space graphs are oriented accordingly. This detail is added because we deal with the "forward" problem of protein folding in our restricted binary collision model. In general, edges of a search space graph need not be oriented. Some unfolding can happen or may even be necessary during protein folding to overcome energy or kinetic barriers in a less artificial environment than our model.

Conformations with unfeasible SSUs are *unfeasible* Conformations and are strictly speaking inaccessible in our search space. With the energy function we use (section 2.7), it is common for unfeasible Conformations to have relatively high amounts of energy. For instance, 1BDD's Conformation (1H, 5H)(3H) which contains the unfeasible SSU(1H, 5H) has the largest energy (Table 2).

2.7 Conformation fitness

A search space becomes a fitness landscape when its nodes are assigned fitness values. Fitness of a Conformation may be defined in several ways. We adopt the linear combination approach used by Yang and Sze [13] and quantify the fitness of a Conformation as the sum of the fitness of its constituent SSUs,

i.e. $F(X) = \sum_{i=0}^{n-1} f(SSU_i)$ where SSU_i is the i^{th} SSU of Conformation X, n is the number of SSUs in X and f

is a function that maps a SSU to a real number.

Energetic fitness. To calculate the energy of a SSU x , Yang and Sze [13] extracted the PDB coordinates of the residues in x and applied the original Rosetta energy function to the extracted coordinates. We do the same but use DeepView's (version 4.1.0) Compute Energy (Force Field) function which is a partial implementation of the GROMOS96 force-field [33], to do the energy calculations. Table 2 lists the energy values of 1BDD's SSUs and Conformations.

Structural fitness. The C_{SCN0} value of a SSU x is the clustering coefficient obtained using only the native shortcuts whose endpoints both belong to residues in x . The C_{SCN0} values for 1BDD's SSUs and Conformations are listed in Table 2.

Table 2 Thermodynamic and structural fitness of 1BDD's SSUs and Conformations.

SSU	Conformation	Energetic fitness (E)		C_{SCN0} fitness	
		SSU	Conformation	SSU	Conformation
(1H)	(1H) (3H) (5H)	25.3863	337.5233	0.4708	1.2089
(3H)	(1H) (3H) (5H)	157.7012	337.5233	0.5026	1.2089
(5H)	(1H) (3H) (5H)	154.4357	337.5233	0.2356	1.2089
(1H 3H)	(1H 3H) (5H)	-244.7240	-90.2885	0.2917	0.5272
(3H 5H)	(3H 5H) (1H)	-222.1320	-196.7460	0.3420	0.8128
(1H 5H)	(1H 5H) (3H)	545.1691	702.8700	0.2620	0.7646
(1H 3H 5H)	(1H 3H 5H)	-271.9150	-271.9150	0.2534	0.2534

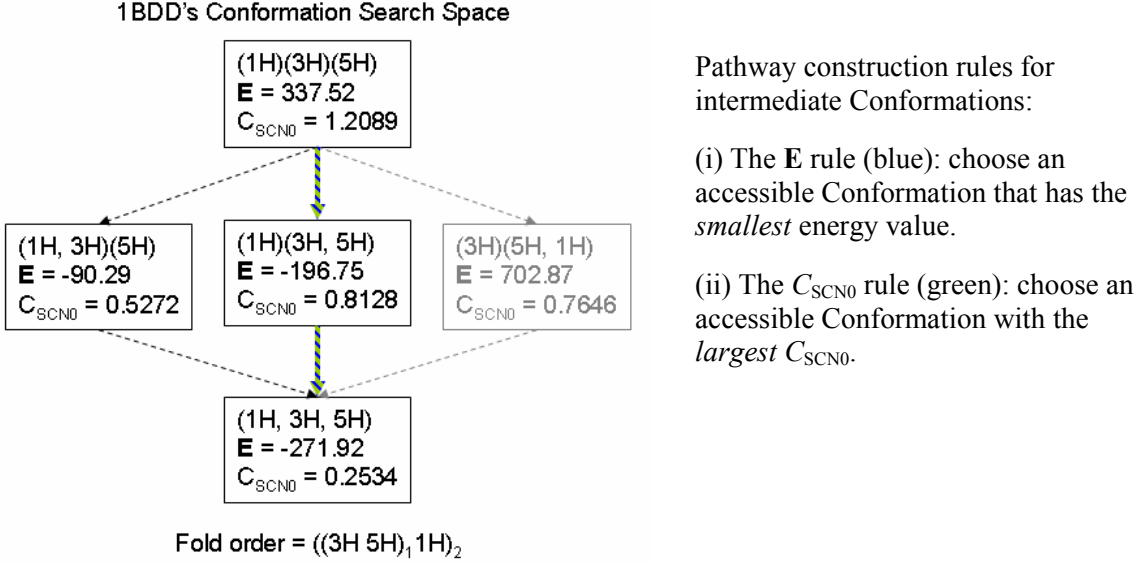


Fig. 4 1BDD's Conformation search space. The arcs denote accessibility between Conformations. Unfeasible and thus inaccessible Conformations are placed in grayed boxes. The C_{SCN0} folding pathway is traced with green arcs while the **E** (steepest descent in energy) folding pathway is traced with blue arcs. In the case of 1BDD, these two folding pathways are identical, and the overlapping portions of the pathways is shown by the blue and green striped arcs.

2.8 Folding pathway identification

A folding pathway is a path in the Conformation search space graph that starts at the Conformation with the maximum number of SSUs and ends at the Conformation with only one SSU. The challenge is to identify a fitness gradient or rule to guide the selection of intermediate Conformations that make a plausible folding pathway for proteins in general.

Yang and Sze [13] approached this challenge by following the path of steepest descent in free-energy. Their pathway construction rule is: choose an accessible Conformation that yields the steepest descent in free-energy at each step. Fig. 4 illustrates the construction of such a folding pathway for 1BDD. Conformation (1H)(3H, 5H) is selected as the intermediate Conformation because it has the *smallest energy value* (**E**) of the feasible Conformations accessible from the Conformation (1H)(3H)(5H).

The pathway construction rule we propose is the following: choose an accessible Conformation with the largest C_{SCN0} at each step. Fig. 4 demonstrates the construction of this folding pathway for 1BDD. Conformation (1H)(3H, 5H) is selected as the intermediate Conformation because it has the *largest* C_{SCN0} value of the feasible Conformations accessible from the Conformation (1H)(3H)(5H). For 1BDD, the C_{SCN0} rule also identifies the folding pathway of steepest descent using the DeepView's energy values. We would like to see whether this agreement holds for the other proteins as well.

3. Results

3.1 Physical basis of shortcut edges

SCN0s represent their respective PRN0s well in terms of secondary structure content. The proportion of PRN0 edges that are short-range is higher in the predominantly helix structured (α -rich) proteins 1MBC, 1BIN, 1BDD and 2F4K (Fig. 5, Table A1). This is expected since helices are formed with short-range contacts, while medium to long-range contacts are required for beta sheets. The proportion of SCN0 edges that are short-range is also higher in the α -rich proteins (Fig. 5). Almost all (>91%) of the native shortcuts in the four α -rich proteins are short-range, while an average of 60% of native shortcuts are short-range in the other proteins (Table A3). Both C_{SCN0} and C_{PRN0} appear to be independent of protein

size (Figs. A2 and A3). However, C_{SCN0} seems more sensitive to fold type (secondary structure composition) than C_{PRN0} (Fig. 6). β -strand rich proteins have perceptibly smaller C_{SCN0} values on average.

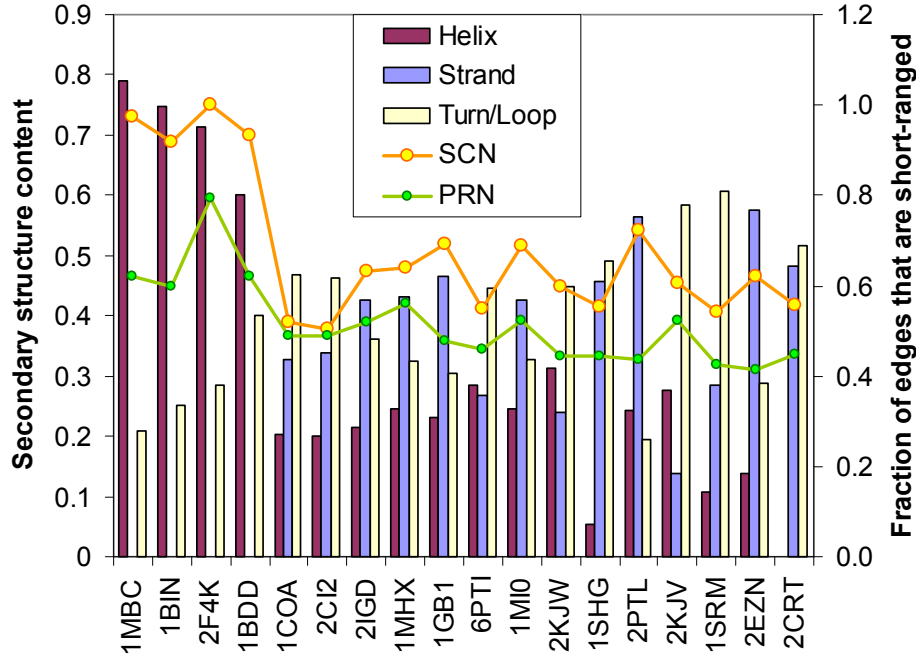


Fig. 5 Secondary structure composition of the 18 proteins (Tables A1 & A3), and their fraction of PRN0 and of SCN0 edges that are short-range.

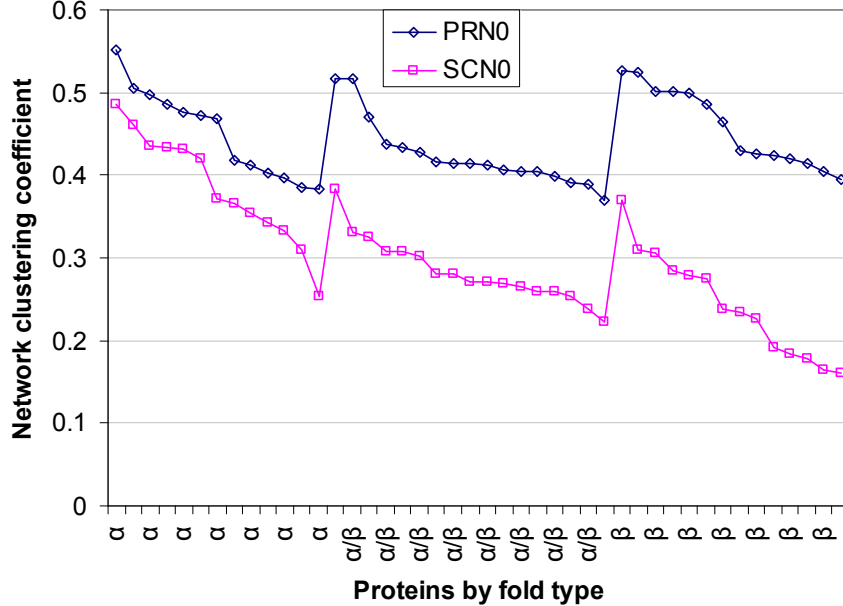


Fig. 6 Network clustering coefficients calculated with PRN0 and with SCN0 edge sets for the 44 proteins in Table A4 arranged by fold type. Fold type appears to be a stronger influence on C_{SCN0} than on C_{PRN0} .

A protein's native state, i.e. its functionally viable state ensemble, may be defined by large kinetic traps or high energy barriers preventing further folding or significant unfolding. Previously, we observed that there is also a structural barrier or topological gap in terms of average C_{PRN} over the native state

ensemble and the average C_{PRN} over non-native state ensembles, for the 2EZN protein [12]. We have since verified that an analogous gap also exists between C_{SCN0} and C_{SCN} for the 2EZN protein.

To perceive what kind of chemical bonds the shortcut edges could represent, the set of hydrogen bonds (*hb*) obtained with HBPlus [31] is compared with several subsets of a protein's PRN0 edges. The edge subsets are: all PRN0 edges (*e*), long-range PRN0 edges (*le*), short-range PRN0 edges (*se*), all SCN0 edges (*sc*) and short-range SCN0 edges (*scse*). For all the 18 proteins examined, all hydrogen bonds identified by HBPlus for a protein are contained within the protein's PRN edge set.

To measure the extent of similarity between the set of hydrogen bonds and each of the edge subsets, we compute the Jaccard Index as $(hb \cap ex) / (hb \cup ex)$ where *ex* is either *e*, *le*, *se*, *sc* or *scse*. We find the shortcut edge sets to be most similar to the hydrogen bond sets (Fig. 7). The Jaccard Index with the shortcut set (*sc_hb*) is significantly (one-sided paired t-test p-value < 0.01) larger than the Jaccard Index with the set of short-range edges (*se_hb*), but not significantly different from the Jaccard Index with the set of short-range shortcut edges (*scse_hb*). Unlike shortcut edges, the hydrogen bonds of the proteins examined create networks with negligible clustering coefficients.

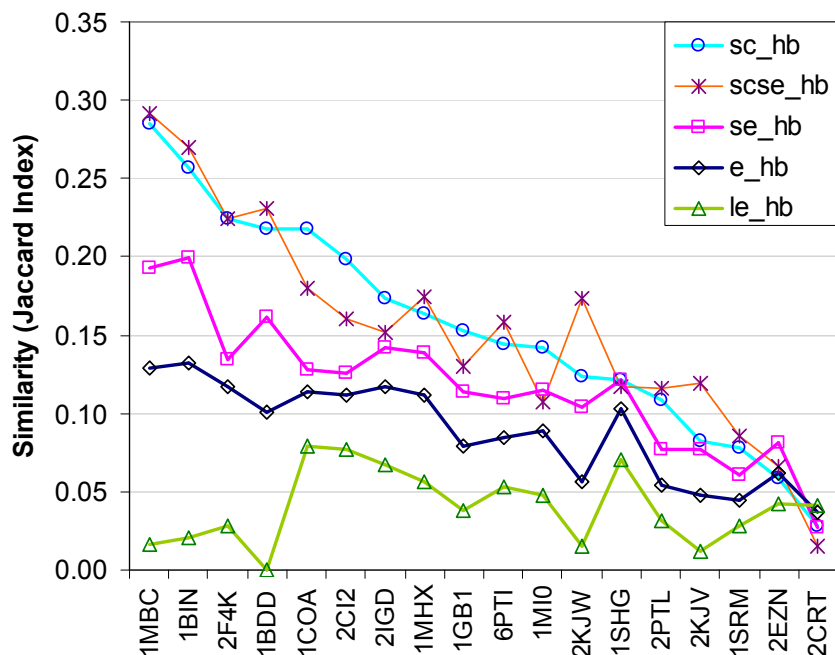


Fig. 7 Similarity (measured by the Jaccard Index) between the set of hydrogen bonds (*hb*) obtained with HBPlus [30] on the (cleaned) PDB file of a protein, and five edge sets: all PRN0 edges (*e*), long-range PRN0 edges (*le*), short-range PRN0 edges (*se*), SCN0 edges (*sc*) and short-range SCN0 edges (*scse*). The shortcut edge sets are the most enriched with hydrogen bonds.

3.2 Relative contact order (RCO) of shortcut edges

A clear evidence of the strong influence a protein's native topology has on the protein folding process is the negative correlation found between relative contact order and folding rates of small proteins [7, 8]. Relative contact order (RCO) = CO/N where *CO* is contact order or average sequence separation of native contacts, and *N* is the number of residues. Other single-value metrics based on native topology have been studied, and they all point to the influence of native-state topology on protein folding rates [40]. We use folding rate $\ln(k_f)$ data from Table 1 of [40] to test whether this relationship extends to PRN0 and SCN0 edges (the 44 PIDs used in this test are listed in Table A4).

We find a significant negative correlation between $\ln(k_f)$ and all three measures of native-state topology: *CO*, *RCO* and $RCO \times N^{0.607}$ [41], for both PRN0 and SCN0 edges (Table 3). The Pearson

correlation is strongest when RCO is scaled with protein size, and SCN0 edges produce stronger correlations than PRN0 edges. The RSC edge sets serve as a null model to the SCN0 edge sets. A RSC is a set of PRN0 edges randomly selected to uniquely replace edges in an SCN0.

Table 3 Pearson's correlation coefficients (ρ) between relative folding rates $\ln(k_f)$ of 44 two-state proteins and three measures of native-state topology: Contact Order (CO), Relative Contact Order (RCO) and RCO scaled with protein chain length N , using three different edge sets.

Native-state topology metric	CO (Fig. A4)			RCO (Fig. A5)			RCO $\times N^{0.607}$ (Fig. A6)		
Edge set	PRN0	SCN0	RSC	PRN0	SCN0	RSC	PRN0	SCN0	RSC
Pearson's ρ	-0.5563	-0.7128	-0.5579	-0.6715	-0.7165	-0.5802	-0.7308	-0.7591	-0.7083
p-value	8.8E-05	5.6E-08	8.3E-05	6.0E-07	4.5E-08	3.6E-05	1.7E-08	2.3E-09	7.4E-08

Fig. 8 is a plot of the PRN0 and SCN0 RCO values for the 18 proteins in Table A1. The α -rich proteins (1MBC, 1BIN, 1BDD and 2F4K) are expected to fold faster than the β -rich proteins (1SRM, 1SHG and 2CRT), and indeed they have smaller PRN0 and SCN0 RCO values, and occupy the lower left quadrant of the plot. The β -rich proteins, which are expected to fold more slowly, tend to congregate in the upper right quadrant.

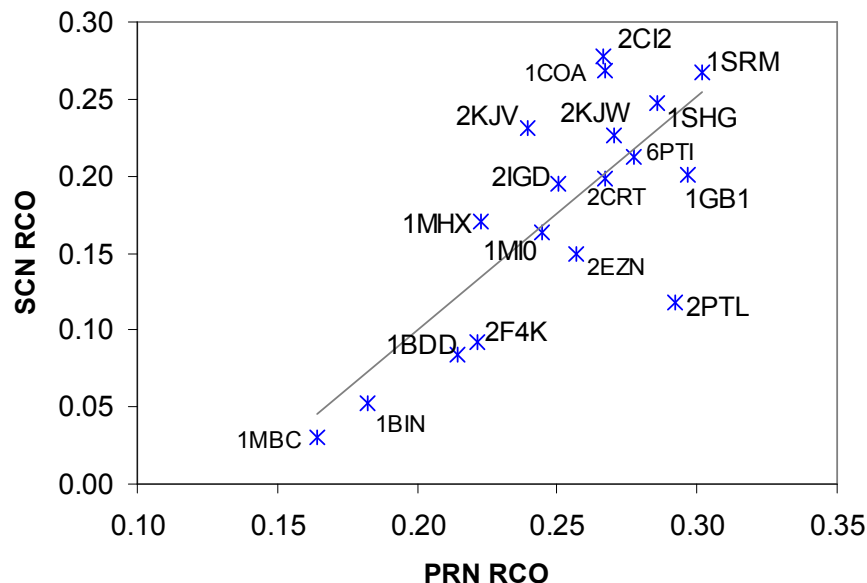


Fig. 8 PRN0 RCO and SCN0 RCO for 18 small proteins.

3.3 Folding pathways and initial reaction points

The folding pathways identified by the C_{SCN0} rule and the **E** rule (section 2.8) with the RBC model are presented in Table B1. These folding pathways are transcribed in the vernacular common in protein literature in Table 4. Search details of these pathways can be found in Appendix B. A folding pathway is described succinctly using a numbered parentheses format. A unique positive integer is associated with each pair of parentheses to record the fold order unambiguously. Elements of SSUs in smaller numbered parentheses combine earlier. For example, $((\beta 1 \beta 2)_1 \alpha 1)_3 (\beta 3 \beta 4)_2)_4$ describes the following sequence of fold events: (i) β -strands $\beta 1$ and $\beta 2$ form SSU($\beta 1 \beta 2$), (ii) β -strands $\beta 3$ and $\beta 4$ form SSU($\beta 3 \beta 4$), (iii) the α -helix $\alpha 1$ and the first β -hairpin form SSU($\beta 1 \beta 2 \alpha 1$), and (iv) finally the second hairpin and SSU($\beta 1 \beta 2 \alpha 1$) form the complete native Conformation SSU($\beta 1 \beta 2 \alpha 1 \beta 3 \beta 4$).

Fig. B7 plots the energy of Conformations on the C_{SCN0} and the **E** folding pathways against their fraction of shortcut edges. Except for 1MHX and 2CI2, the C_{SCN0} folding pathways are identical to their respective **E** folding pathways. The deviations are not without good reason as explained below. Except

for 1MHX and 1MI0 for whom energy increases in both the C_{SCN0} and the **E** folding pathways in the final step(s), the C_{SCN0} and the **E** folding pathways are energetically favourable, i.e. energy decreases with each fold step as the search approaches the native conformation. This behavior is consistent with the funnel shaped folding energy landscape model for small proteins.

The number of hydrogen bonds in Conformations on the C_{SCN0} folding pathways increases monotonically as the search progresses (Fig. B8). Hydrogen bonds play a critical directional role in main-chain interactions, and are important stabilizers of secondary structures.

Table 4 Protein folding pathways identified by C_{SCN0} and by **E** with the RBC model. Yang & Sze folding pathways [13] are provided for reference where available. 'same' denotes that the pathway is identical to the one in the previous column on the left.

PDB ID	C_{SCN0} folding pathway	E folding pathway	Yang & Sze's folding pathway
1BDD	$(\alpha 1 (\alpha 2 \alpha 3)_1)_2$	same	same
2IGD	$((\beta 1 \beta 2)_2 (\alpha 1 (\beta 3 \beta 4)_1)_3)_4$	same	Not applicable.
1GB1	$((\beta 1 \beta 2)_2 (\alpha 1 (\beta 3 \beta 4)_1)_3)_4$	same	$((\alpha 1 (\beta 3 \beta 4)_1)_2 \beta 1)_3 \beta 2)_4$
2PTL	$((\beta 1 \beta 2)_1 \alpha 1)_3 (\beta 3 \beta 4)_2)_4$	same	$((\beta 3 \beta 4)_2 (\beta 1 \beta 2)_1)_3 \alpha 1)_4$
1MHX	$((\beta 1 \beta 2)_1 \alpha 1)_3 (\beta 3 \beta 4)_2)_4$	$((\beta 1 \beta 2)_2 \alpha 1)_3 (\beta 3 \beta 4)_1)_4$	$((\beta 3 (\beta 4 (\beta 1 \beta 2)_1)_2)_3 \alpha 1)_4$
1MI0	$((\beta 1 \beta 2)_1 (\alpha 1 (\beta 3 \beta 4)_2)_3)_4$	same	$((\beta 3 (\beta 4 (\beta 1 \beta 2)_1)_2)_3 \alpha 1)_4$
2CI2	$((\beta 1 \alpha 1)_3 ((\beta 2 \beta 3)_1 \beta 4)_2)_4$	$(\beta 1 ((\alpha 1 (\beta 2 \beta 3)_1)_2 \beta 4)_3)_4$	$(\beta 1 ((\alpha 1 (\beta 2 \beta 3)_1)_2 \beta 4)_3)_4$

1BDD is the B domain of *Staphylococcal* protein A. Its secondary structure comprises three helices (Fig. 2). 1BDD is an almost symmetric protein, which prompts questions about how the symmetry is broken during (un)folding, and the possibility of multiple highly populated (un)folding pathways under different conditions [42]. While experiments and simulations concur that the middle α -helix ($\alpha 2$) is the most stable structure, there is disagreement about the sequence of fold events involving the first and third α -helices in the transition state [42, 43]. The C_{SCN0} folding pathway for 1BDD is identical to the folding pathway predicted by Yang & Sze [13] and by COMMA [28]. This pathway is the dominant unfolding pathway passing through TS2 under condition of high temperature or high denaturant concentration [42]. A non-random choice between the two possible folding routes for 1BDD could not be made with a simple count of native shortcuts since both Conformations (1H 3H)(5H) and (1H)(3H 5H) have the same number of shortcuts (Table C1). The alternative folding pathway that passes through TS1 in [42], which is supported by experiments but hard to simulate, could be selected using a different rule since Conformation (1H 3H)(5H) boasts more native PRN edges and also more hydrogen bonds than Conformation (1H)(3H 5H) (Table C1). However, these candidate alternative rules do not generalize well, as they quickly break down when the next set of four proteins are considered.

2IGD and 1GB1 are two PDB entries for the B1 immunoglobulin binding domain of *Streptococcal* protein G. They are composed of one α -helix packed against a four-stranded β -sheet comprising two β -hairpins (Figs. B1 and B2). 2IGD and 1GB1 have identical C_{SCN0} and **E** folding pathways, and their C_{SCN0} and **E** folding pathways coincide with each other, but not with Yang and Sze's folding pathway (due to differences in energy function). Nonetheless, all the folding routes in Table 4 for 2IGD and 1GB1 agree that folding begins with the formation of the C-terminal β -hairpin $\beta 3$ - $\beta 4$, consistent with literature [9].

2PTL is the B1 immunoglobulin binding domain of *Peptostreptococcal* protein L. It is also composed of one α -helix packed against a four-stranded β -sheet comprising two β -hairpins (Fig. B3). Its C_{SCN0} and **E** folding pathways coincide with each other, but not with Yang and Sze's folding pathway. Nonetheless, all the folding routes in Table 4 for 2PTL agree that folding begins with the formation of the N-terminal β -hairpin $\beta 1$ - $\beta 2$, consistent with literature [44].

1MHX and 1MI0 (Figs. B4 and B5) are crystallized structures of the NuG1 and NuG2 variants of protein G [45]. These variants were created by searching for a replacement sequence in the first (N-terminal) β -hairpin of protein G that would increase its stability. Accordingly, the native Conformations of both 1MHX and 1MI0 have lower energy than the native 1GB1 Conformation (Fig. B7). NuG1 and

NuG2 also fold much faster than protein G [45]. In Fig. 8, we find both 1MHX and 1MI0 situated to the bottom and left of 1GB1. (Here is an example where increased native-state stability, increases folding rate and reduces RCO.) All except one of the folding routes in Table 4 for 1MHX and 1MI0 agree that folding begins with the formation of the N-terminal β -hairpin β 1- β 2. The exception is 1MHX's **E** folding pathway which proposes the second β -hairpin instead, which runs contrary to literature [45].

Results from the set of four structurally similar proteins just discussed support the applicability of C_{SCN0} , a structural metric based on native-state topology, to the protein folding pathway problem. In all four cases, C_{SCN0} correctly identified the expected initial reaction point. Interestingly, the 1MHX case shows that the choice made with C_{SCN0} can deviate from the **E** folding pathway in a positive manner, and can lead to a smaller energy barrier to the native state (Fig. B7). The correct initial reaction point for these four proteins could not be reproduced with C_{PRN0} (Table C2), the number of hydrogen bonds (Table C3), a random subset of PRN edges (Table C4) or SSE communication strength (Table C7).

Other than the initial reaction point, the C_{SCN0} folding pathways do not agree generally with Yang and Sze's folding pathways. The fold events on the C_{SCN0} pathways for the four proteins are quite regimented. First, the two β -hairpins are formed one after the other, then the α -helix joins one of the β -hairpins (usually the one that formed first), and finally the other β -hairpin is included. These fold substructures are requisite folding elements on low ECO routes for proteins G and L [38], and coincide also with substructures in the formation order suggested by rigidity analysis [46]. Formation of β -hairpins in folding transition states are attractive since native contacts can be satisfied with minimal loss in chain entropy [44]. In contrast, the fold events on Yang and Sze's pathways for this set of four proteins are more diverse, and all involve an intermediate Conformation that is unfeasible in our RBC model. However, support for pairing of the first and fourth β -strands to form a three-stranded β -sheet in the transition state has been documented for both proteins G and L [9, 22, 24].

Why do structurally similar proteins fold differently? A number of material and structural causes have been proposed, including differences in protein sequence⁴ [41], energetics [9, 22], contact density⁵ [9] and structural rigidity [46]. We examined the density of both SCN0 and PRN0 edges in feasible SSUs at the initial fold step for all four proteins (Tables C5 and C6). In agreement with ref. [9], the second β -hairpin of protein G has higher contact density than the first β -hairpin. However, this asymmetry in native contact density (at least in our PRN0 and SCN0 models) is also true for protein L, NuG1 and NuG2. Hence contact density of SSUs cannot be relied upon to identify initial folding reaction points consistently. And neither can a rule based on energetics (at least with the potential energy function we used) of SSUs (Table C8). The **E** rule, which is based on energy of Conformations, incorrectly identified the second β -hairpin as the initial reaction point for 1MHX.

2CI2 is the Chymotrypsin Inhibitor 2 protein. It has one α -helix, a reactive site loop and a six-stranded β -sheet (which is sometimes simplified to four) (Fig. B6). Its **E** folding pathway coincides with Yang and Sze's folding pathway, and the low fold order of SSU(α 1 (β 2 β 3)), reflects the early formation of the hydrophobic core by its nucleus residues. The C_{SCN0} folding pathway is more similar to the folding route suggested in [38] where folding clusters β 2- β 3 and β 3- β 4 are requisite substructures for a low ECO-route. Nonetheless, all the 2CI2 pathways in Table 4 agree with results from experiments and simulations that folding is instigated by the β 2- β 3 substructure (or β 3- β 4 if dealing with the six-strands of the β -sheet) [23, 34].

3.4 Identifying key residues for protein folding with PRN0

Ref. [46] examined the structural rigidity of proteins GB1, LB1, NuG1 and NuG2 in terms of their degrees of freedom in the pebble game, and found that in all four cases, the more rigid β -hairpin is the

⁴ Their simulation study was unable to reproduce experimental results for proteins G and L. Since they used a model that does not consider sequence specific information, the explanation for the discrepancy between experiment (laboratory) and simulation results is sequence specific information.

⁵ The presence of two GLY amino acids in the first β -hairpin, which reduces side-chain interactions, contributes to the difference in contact density between the two β -hairpins.

one that forms earlier. Another way of gauging protein structural rigidity which makes use of basic network characteristics such as node degree and node clustering directly appeared in ref. [47]. Nodes with larger degrees (more globally connected) and smaller clustering coefficients (less locally connected) are deemed more rigid. Using published data on 1BDD, 2IGD, 1GB1, 2PTL and 2CI2, we observe that residues purported to form a protein's "folding nucleus", i.e. those residues involved in stable long-range native interactions in the denatured or transition states, tend to be more rigid. The large connectivity (node degree) of key folding residues is not surprising since they are frequently buried in the (extended) hydrophobic core of proteins.

For this analysis, we find that we need to use PRN0 and not SCN0 network statistics to produce meaningful results. Fig. D1 gives a sense of why this is. It plots burial of src SH3 domain residues in the native state (Burial data taken from Table 1 of ref. [48]) against 1SRM's PRN0 and SCN0 node degrees and node clustering coefficients. The PRN0 network statistics are more strongly correlated with burial of residues than the SCN0 network statistics. Node degree is strongly and positively correlated with burial; while node clustering is weakly negatively or not correlated at all with burial.

Occasionally we refer to key folding residues as nucleation sites or the nucleus. However, this is not an assertion that the folding mechanism is nucleation-condensation. The key folding residues listed below are identified through one or more of the following methods in the references: CABS simulation [23, 24, 43], coarse-grain Brownian dynamics simulation combined with protein sequence alignment to identify residues with large force constants that are also conserved within a protein fold (Suppl. Mat. for ref. [25]), and hydrogen-deuterium exchange (H-X) (Table 1 in ref. [49]). These three key folding residue sets may overlap with each other. We refer to the conserved rigid residues tagged in [25] as mechanically rigid (M-R) sites. For 2IGD and 1SRM, we use the provided data for 1IGD and 1SRL, respectively. The M-R sites confer structural stability in a protein's native state, but many of these sites also coincide with folding nuclei identified in the literature. The H-X sites include amide protons (NHs) which are slowest to exchange out, or first to gain protection. The H-X probes do not identify nucleation sites per se, but rather the neighborhood where they might be found. Key folding sites on turns (which are crucial to trigger β -hairpin formation) are not detected.

1BDD (Fig. D2) Residues involved in frequently formed contacts in the transition state structures between the first and second helices (1H-3H) are: F14, L18, F31, I32 and L35; and between the second and third helices (3H-5H) are: L45, F31 and L35 [43]. The H-X sites are Y15...L18, R28, L35, K36, A49, K50 and K51. Except for L18 which is a turn residue immediately after 1H, the key folding residues congregate on the three α -helices.

2IGD (Fig. D3) The M-R sites are Y8, L10, A31, F35, F57 and V59. These sites are located on the first and forth β -strands (1S and 9S), and the α -helix (5H). Key folding residues are absent on both the second and third β -strands (3S and 7S). The remaining four most rigid residues in Fig. D3 belong to 1S, 5H, 6T and 7S. The residue on the third β -strand (7S) is W48, which makes shortcut edges with residues F57, T58 and V59, which are on the forth (9S). This network of shortcut edges may help explain the propensity for the second β -hairpin (comprising 7S and 9S), to form more quickly, as indicated in our C_{SCN0} folding pathway for 2IGD.

1GB1 (Fig. D4) The folding nucleation sites are Y3, L5, F30, W43, Y45 and F52 [24]. These six residues are evolutionarily conserved in protein G-like folds, and make frequent long-range native interactions with K4, I6, L7, A26, T51, T53 and V54 as part of the nucleation growth process in simulations (Table 1 in ref. [24]). The H-X sites are L5, I6, T25, A26, E27, F30, T44, K50, and T51...V54. Except for K50 which is a turn residue immediately before 8S, the key folding residues congregate on the first, third and forth β -strands (0S, 6S and 8S), and the α -helix (4H).

2PTL (Fig. D5) The H-X sites are I20, A22, L24, I25, F36, S45, A47...D52, L72, I74, and K75. The key folding residues congregate on the first, second and forth β -strands (0S, 2S and 8S), and the α -helix (4H). Interestingly, for both 1GB1 and 2PTL, key folding residues are absent on one of the β -strands of the β -hairpin that forms later, i.e. 2S for 1GB1, and 6S for 2PTL.

2CI2 (Fig. D6) The folding nucleation sites for 2CI2 are A35, I39, V66, L68 and I76 [23, 34]. Four of these sites (A35, I39, V66, L68), together with R67 and P80 are M-R sites. The H-X sites are K30, I39,

L40, I49, L51, V66, L68, F69 and V70. Except for K30, I76, and P80, the key residues congregate on the α -helix (3H), and the second and third β -strands (5S and 7S). K30 is a turn residue immediately before the helix (3H), I76 is a residue in the turn (8T) between the third and forth β -strands (7S and 9S), and P80 is a residue in the forth β -strand (9S). Key folding residues are absent from the first β -strand (1S), which only gets involved at the later stages in our C_{SCN0} folding pathway for 2CI2.

Attempts at identifying key folding residues using characteristics of protein structure networks exist, e.g. [50] and [51]. The results in this section serve to support our C_{SCN0} folding pathways (Table 4), and for now, are considered more descriptive than predictive.

4. Conclusion

We have shown the relevance and applicability of a protein's ShortCut Network (SCN) to the protein folding problem, but more remains to be done. The results point to shortcut edges as a meaningful subset of native contacts, which could bring us closer to answer the question what exactly about a protein's native-state topology that contributes to its successful folding into a unique native state, and to a precise definition of a protein's native-state topology.

Acknowledgements

This work was made possible by the facilities of the Shared Hierarchical Academic Research Computing Network (SHARCNET:www.sharcnet.ca) and Compute/Calcul Canada. Thanks to the DYNAMIOMICS group for the 2EZN MD dataset and to C.N. Rowley for helpful discussions.

References

- [1] Dill KA and MacCallum JL (2012) The protein-folding problem, 50 years on. *Science* 338:1042-1046.
- [2] Levinthal, C. (1969) How to fold gracefully. In: Debrunner, J.T.P., and Munck, E. (eds.) *Mossbauer Spectroscopy in Biological Systems: Proceedings of a Meeting held at Allerton House, Monticello, Illinois.* University of Illinois Press, pp. 22-24.
- [3] Dill KA and Chan HS (1997) From Levinthal to pathways to funnels. *Nature Structural Biology* 4(1):10-19.
- [4] Karplus M (1997) The Levinthal paradox: yesterday and today. *Folding & Design* 2, pp. S69-S75.
- [5] Englander SW and Mayne L (2014) The nature of protein folding pathways. *PNAS* 111(45):15873-15880.
- [6] Alm E and Baker D (1999) Matching theory and experiment in protein folding. *Current Opinion in Structural Biology* 9(2):186-196.
- [7] Plaxco KW, Simons KT and Baker D (1998) Contact order, transition state placement and the refolding rates of single domain proteins. *J. Mol. Biol.* 277:985-994.
- [8] Plaxco KW, Simons KT, Ruczinski I and Baker D (2000) Topology, stability, sequence and length: Defining the determinants of two-state protein folding kinetics. *Biochemistry* 39(37):11177-11183.
- [9] McCallister EL, Alm E and Baker D (2000) Critical role of β -hairpin formation in protein G folding. *Nature Structural Biology* 7(8):669-673.
- [10] Nickson AA and Clarke J (2010) What lessons can be learned from studying the folding of homologous proteins? *Methods* 52:38-50.
- [11] Nickson AA, Wensley BG and Clarke J (2013) Take home lessons from studying related proteins. *Current Opinion in Structural Biology* 23:66-74.
- [12] Khor S (2016) Protein residue networks from a local search perspective. *Journal of Complex Networks* 4(2):245-278.
- [13] Yang Q and Sze SH (2008). Predicting protein folding pathways at the mesoscopic level based on native interactions between secondary structure elements. *BMC Bioinformatics* 9:230.

- [14] Alm E and Baker D (1999) Prediction of protein-folding mechanisms from free-energy landscapes derived from native structures. *Proc. Natl. Acad. Sci. USA* 96:11305-11309.
- [15] Anfinsen CB (1973) Principles that govern the folding of protein chains. *Science* 181(4096):223-230.
- [16] Sohl JL, Jaswal SS and Agard DA (1998) Unfolded conformations of a-lytic protease are more stable than its native state. *Nature* 395:817-819.
- [17] Im H, Ahn H-Y and Yu M-H (2000) Bypassing the kinetic trap of serpin protein folding by loop extension. *Protein Science* 9:1497-1502.
- [18] Berman HM, Westbrook J, Feng Z, Gilliland G, Bhat TN, Weissig H, Shindyalov IN and Bourne PE (2000). The Protein Data Bank. *Nucleic Acids Research* 28: 235-242. <http://www.rcsb.org/pdb>
- [19] Chatterjee S, Ghosh S and Vishveshwara, S (2013) Network properties of decoys and CASP predicted models: a comparison with native protein structures. *Mol. BioSyst.* 9:1774-1788.
- [20] Kannan N and Vishveshwara S (1999) Identification of side-chain clusters in protein structures by a graph spectral method. *J. Mol. Biol.* 292:441-464.
- [21] Honig B and Cohen FE (1996) Adding backbone to protein folding: why proteins are polypeptides. *Folding & Design* 1:R17-R20.
- [22] Clementi C, Garcia AE and Onuchic JN (2003) Interplay among tertiary contacts, secondary structure formation and side-chain packing in the protein folding mechanism: All-atom representation study of protein L. *J. Mol. Biol.* 326:933-954.
- [23] Kmiecik S and Kolinski A (2007) Characterization of protein-folding pathways by reduced-space modeling. *PNAS* 104(30):12330-12335.
- [24] Kmiecik S and Kolinski A (2008) Folding pathway of the B1 domain of protein G explored by multiscale modeling. *Biophysical J.* 94:726-736.
- [25] Sacquin-Mora S (2015) Fold and flexibility: what can proteins' mechanical properties tell us about their folding nucleus? *J. R. Soc. Interface* 12:20150876.
- [26] Khor S (2016) Comparing local search paths with global search paths on protein residue networks: allosteric communication. *Journal of Complex Networks* doi: 10.1093/comnet/cnw020
- [27] Cheung MS, Chavez LL and Onuchic JN (2004) The energy landscape for protein folding and possible connections to function. *Polymer* 45:547-555
- [28] Karami Y, Laine E and Carbone A (2016) Dissecting protein architecture with communication blocks and communication segment pairs. *BMC Bioinformatics* 17(Suppl 2):13.
- [29] Kleinberg J (2000) Navigation in a small world. *Nature* 406:845.
- [30] Humphrey W, Dalke A and Schulten K (1996) VMD - Visual Molecular Dynamics. *J. Molec. Graphics*, 14: 33-38. <http://www.ks.uiuc.edu/Research/vmd/>
- [31] McDonald IK and Thornton JM (1994) Satisfying hydrogen bonding potentials in proteins. *J. Mol. Biol.* 238(5):777-793. <http://www.ebi.ac.uk/thornton-srv/software/HBPLUS/>
- [32] Watts DJ and Strogatz SH (1998) Collective dynamics of 'small-world' networks. *Nature* 393, 440-442.
- [33] Guex N and Peitsch MC (1997) SWISS-MODEL and the Swiss-PDBViewer: An environment for comparative protein modeling. *Electrophoresis* 18:2714-2723. <http://www.expasy.org/spdbv/>
- [34] Itzhaki LS, Otzen DE and Fersht AR (1995) The structure of the transition state for folding of Chymotrypsin Inhibitor 2 analyzed by protein engineering methods: Evidence for a nucleation-condensation mechanism for protein folding. *J. Mol. Biol.* 254:260-288.
- [35] Nolting B and Andert K (2000) Mechanism of protein folding. *Proteins* 41:288-298
- [36] Gianni S, et al. (2003) Unifying features in protein-folding mechanisms. *PNAS* 100(23):13286-13291.
- [37] Fiebig KM and Dill KA (1993) Protein core assembly processes. *J. Chem. Phys.* 98(4):3475-3478.
- [38] Weikl TR and Dill KA (2003) Folding rates and low-entropy-loss routes of two-state proteins. *J. Mol. Biol.* 329:585-598.

- [39] Munoz V and Eaton WA (1999) A simple model for calculating the kinetics of protein folding from three-dimensional structures. *PNAS* 96:11311-11316.
- [40] Zou T and Ozkan SB (2011) Local and non-local native topologies reveal the underlying folding landscape of proteins. *Phys. Biol.* 8:066011.
- [41] Koga N and Takada S (2001) Roles of native topology and chain-length scaling in protein folding: A simulation study with a Gō-like model. *J. Mol. Biol.* 313:171-180.
- [42] Itoh K and Sasai M (2006) Flexibly varying folding mechanism of a nearly symmetrical protein: B domain of protein A. *PNAS* 103(19):7298-7303.
- [43] Kmiecik S, Gront D, Kouza M and Kolinski A (2012) From coarse-grained to atomic-level characterization of protein dynamics: Transition state for the folding of B domain of protein A. *J. Phys. Chem. B* 116:7026-7032.
- [44] Kim DE, Fisher C and Baker D (2000) A breakdown of symmetry in the folding transition state of protein L. *J. Mol. Biol.* 298:971-984.
- [45] Nauli S, Khulman B, Le Trong I, Stenkamp RE, Teller D and Baker D (2002) Crystal structures and increased stabilization of the protein G variants with switched folding pathways NuG1 and NuG2. *Protein Science* 11:2924-2931.
- [46] Thomas S, Tang X, Tapia L and Amato NM (2007) Simulating protein motions with rigidity analysis. *J. Comp. Biol.* 14(6):839-855.
- [47] Piazza F and Sanejouand Y-H (2008) Discrete breathers in protein structures. *Physical Biology* 5, 026001.
- [48] Riddle DS, Grantcharova VP, Santiago JV, Alm E, Ruczinski I and Baker D (1999) Experiment and theory highlight role of native state topology in SH3 folding. *Nat. Struc. Biol.* 6(11):1016-1024.
- [49] Li R and Woodward C (1999) The hydrogen exchange core and protein folding. *Prot. Sci.* 8:1571-1591.
- [50] Vendruscolo M, Dokholyan NV, Paci E and Karplus M (2002) Small-world view of the amino acids that play a key role in protein folding. *Phys. Rev. E* 65:061910
- [51] Li J, Wang J and Wang W (2008) Identifying folding nucleus based on residue contact networks of proteins. *Proteins* 71:1899-1907.

Appendix A Materials and Methods

Table A1 Description of 18 proteins used in this study.

PDB ID	Chain	Residue range	Secondary structure			Protein description
			H	S	T	
1MBC	A	1...153	121	0	32	Carbon-monooxy (FE 11)-Myoglobin
1BIN	A	1...143	107	0	36	Leghemoglobin A
1BDD	A	1...60	36	0	24	BdpA: Immunoglobulin-binding B domain of protein A
2F4K	A	42...76	25	0	10	Chicken Villin Subdomain HP-35, K65(NLE, N68H, K70(NLE))
1COA	I	20...83	13	21	30	Chymotrypsin Inhibitor 2
2CI2	I	19...83	13	22	30	Serine proteinase inhibitor (Chymotrypsin) CI-2 from barley seeds
6PTI	A	1...56	16	15	25	Bovine pancreatic proteinase inhibitor (Trypsin)
2IGD	A	1...61	13	26	22	Protein G Igg-Binding domain
1GB1 (Model 1)	A	1...56	13	26	17	GB1: Immunoglobulin-binding domain of Streptococcal protein G
1MHX	A	1...65	16	28	21	NuG1: Redesigned B1 domain of protein G
1MI0	A	1...61	15	26	20	NuG2: Redesigned B1 domain of protein G
2PTL (Model 1)	A	17...78	15	35	12	LB1: Immunoglobulin light-chain binding domain of protein L
2EZN (Model 1)	A	1...101	14	58	29	HIV-Inactivating protein Cyanovirin-N
2CRT	A	1...60	0	29	31	Cardiotoxin III from Taiwan cobra
1SHG	A	6...62	3	26	28	α -spectrin SH3 domain
1SRM (Model 1)	A	9...64	6	16	34	src Tyrosine Kinase SH3 domain
2KJV	A	1...101	28	14	59	Ribosomal protein S6 (Wild-type)
2KJW	A	1...96	30	23	43	Ribosomal protein S6 (permutant P54-55)

Table A2 Secondary structure elements (SSEs) for the seven proteins whose folding pathways are identified by RBC in section 3.3.

PDB ID	SSEs listed from N- to C- termini for RBC	Common descriptors of the non-Turn SSEs
1BDD	0T 1H 2T 3H 4T 5H 6T	$\alpha 1, \alpha 2, \alpha 3$
2IGD	0T 1S 2T 3S 4T 5H 6T 7S 8T 9S	$\beta 1, \beta 2, \alpha 1, \beta 3, \beta 4$
1GB1	0S 1T 2S 3T 4H 5T 6S 7T 8S	$\beta 1, \beta 2, \alpha 1, \beta 3, \beta 4$
1MHX	0T 1S 2T 3S 4T 5H 6T 7S 8T 9S 10T	$\beta 1, \beta 2, \alpha 1, \beta 3, \beta 4$
1MI0	0T 1S 2T 3S 4T 5H 6T 7S 8T 9S 10T	$\beta 1, \beta 2, \alpha 1, \beta 3, \beta 4$
2PTL	0S 1T 2S 3T 4H 5T 6S 7T 8S 9T	$\beta 1, \beta 2, \alpha 1, \beta 3, \beta 4$
2CI2	0T 1S 2T 3H 4T 5S 6T 7S 8T 9S	$\beta 1, \alpha 1, \beta 2, \beta 3, \beta 4$

For 1GB1, 1MHX, 1MI0, 2PTL and 2CI2, we adopt the SSE delineations in [13] (faculty.cs.tamu.edu/shsze/ssfold) but we renamed them so that xSS represents the x^{th} SSE with x starting at 0 for the first SSE at the N-terminus, and SS represents the type of SSE.

For 1BDD and 2IGD, the SSE delineations are as follows (residues belonging to a SSE are in parentheses): the SSEs for **1BDD** are: 0T (1...9), 1H (10...17), 2T (18...24), 3H (25...37), 4T (38...41), 5H (42...56), and 6T (57...60); and the SSEs for **2IGD** are: 0T (1...5), 1S (6...13), 2T (14...17), 3S (18...24), 4T (25...27), 5H (28...40), 6T (41...46), 7S (47...51), 8T (52...55) and 9S (56...61).

Table A3 Several basic characteristics of the 18 native Protein Residue Networks (PRN0) and their respective native Shortcut Network (SCN0).

PDB ID	PRN0						SCN0						
	N	M	$ SE /M$	Mean SD	Max SD	Max ED	N_{SCN}	$ SC $	$ SC /N$	$ SCSE / SC $	Mean SD	Max SD	Max ED
1MBC	153	999	0.621	25.16	136	14.621	152	245	1.60	0.976	4.65	125	9.440
1BIN	143	912	0.600	26.08	134	14.277	143	222	1.55	0.919	7.56	80	9.509
1BDD	60	437	0.622	12.86	41	14.249	58	90	1.50	0.933	5.02	36	9.361
2F4K	35	222	0.793	7.76	34	14.882	35	56	1.60	1.000	3.21	6	8.614
1COA	64	351	0.490	17.11	62	13.480	61	100	1.56	0.520	17.20	61	8.823
2CI2	65	359	0.487	17.34	62	13.390	60	93	1.43	0.505	18.09	61	8.961
6PTI	56	318	0.459	15.52	55	12.631	55	84	1.50	0.548	11.87	35	9.162
2IGD	61	317	0.517	15.29	49	13.311	61	98	1.61	0.633	11.91	48	8.888
1GB1	56	407	0.477	16.62	50	13.490	56	104	1.86	0.692	11.26	48	8.845
1MHX	65	306	0.559	14.48	49	12.944	60	94	1.45	0.638	11.04	48	9.626
1MI0	61	349	0.524	14.92	50	13.756	59	90	1.48	0.689	9.98	48	8.498
2PTL	62	484	0.436	18.10	54	14.149	62	97	1.56	0.722	7.33	23	8.917
2EZN	101	837	0.413	25.91	100	16.416	100	201	1.99	0.622	15.04	90	9.689
2CRT	60	385	0.447	16.02	58	12.416	56	95	1.58	0.558	11.91	36	9.492
1SHG	57	321	0.442	16.30	55	13.949	56	96	1.68	0.552	14.10	54	9.420
1SRM	56	408	0.424	16.91	55	13.840	55	107	1.91	0.542	14.94	54	9.388
2KJV	101	667	0.514	24.21	92	14.117	97	169	1.67	0.609	23.38	90	10.450
2KJW	96	775	0.435	25.97	95	15.673	95	167	1.74	0.599	21.77	88	9.847

Notes:

PRN0 is the Protein Residue Network constructed with native state coordinates. These coordinates are based on the PDB file with some modifications for 1MHX and 1MI0, which were necessary for energy calculations by PDB-Viewer [33].

SCN0 is the shortcut network of a PRN0.

N = number of nodes (amino acids) in a PRN. M = number of edges in a PRN.

SE = set of short-range edges in a PRN. An edge connecting residues x and y is short-range if $|x - y| \leq 10$.

$|SE|$ = cardinality of SE. $|SE|/M$ = fraction of PRN edges which are short-range.

N_{SCN} = number of nodes in a SCN.

SC = set of shortcut edges in a PRN. $|SC|$ = number of edges in a SCN.

SCSE = SCN edges which are short-range; $|SCSE|/|SC|$ = fraction of shortcut edges which are short-range.

SD = sequence separation for a pair of residues (x, y), i.e. $|x - y|$. Mean SD = contact order.

Max SD = maximum sequence separation over all edges in a network.

Max ED = maximum C α -C α Euclidean distance over all edges in a network.

Table A4 The 44 two-state proteins from Table 1 [40] by secondary structure content.

Structure	PIDs
α	1AYI, 1BA5, 1BDD, 1ENH, 1HRC, 1IDY, 1IMQ, 1L8W-A(52...92,113...342), 1LMB-3(6...92), 1PRB, 1VII, 256B, 2A3D
α/β	1APS, 1BF4, 1CIS, 1COA, 1E65-A, 1FKB, 1HZ6-A(2...64), 1LOP, 1POH, 1RIS, 1SPR-A, 1UBQ, 1URN, 2ACY, 2CI2, 2PTL, 2VIK
β	1C8C, 1CSP, 1K8M, 1MJC, 1NYF, 1PKS, 1QTU, 1RLQ(9...64), 1SHF-A, 1SHG, 1SRL, 1TEN-A(803...891), 1WIT, 2VKN

Notes:

These 44 proteins were selected on the basis that their relevant residue ranges could be easily identified from their PDB files, and that their PRNs form a single component which facilitates the identification of shortcut edges.

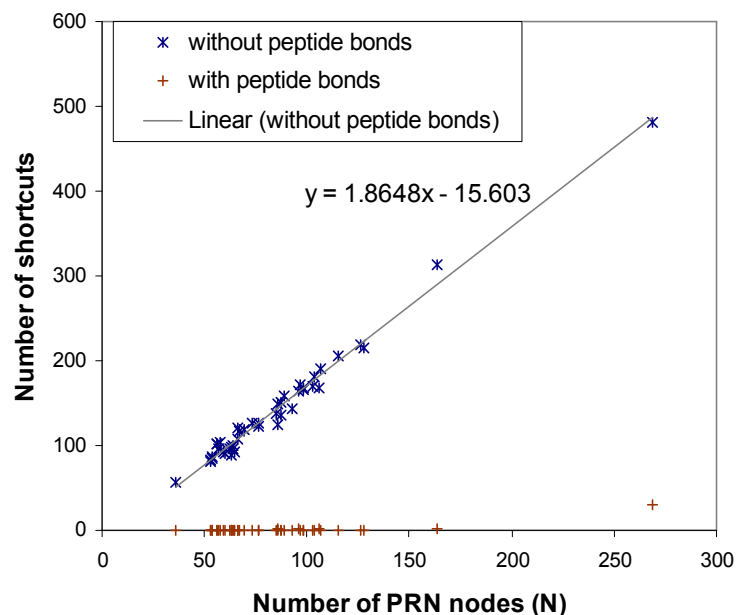


Fig. A1 Number of shortcuts discovered by EDS on PRNs constructed with and without peptide bonds. When peptide bonds are excluded (which is the normal case), the 44 proteins in Table A4 exhibit the familiar $\sim 2N$ relationship [12] between number of shortcut edges and protein chain length, N . This scaling behavior, hydrogen-bond enrichment of shortcut edge sets, EDS's reliance on the position of a protein's $C\alpha$ atoms, and the disruptive effect peptide bonds have on the number of shortcuts suggest that shortcut edges are capturing information about a protein's backbone geometry.

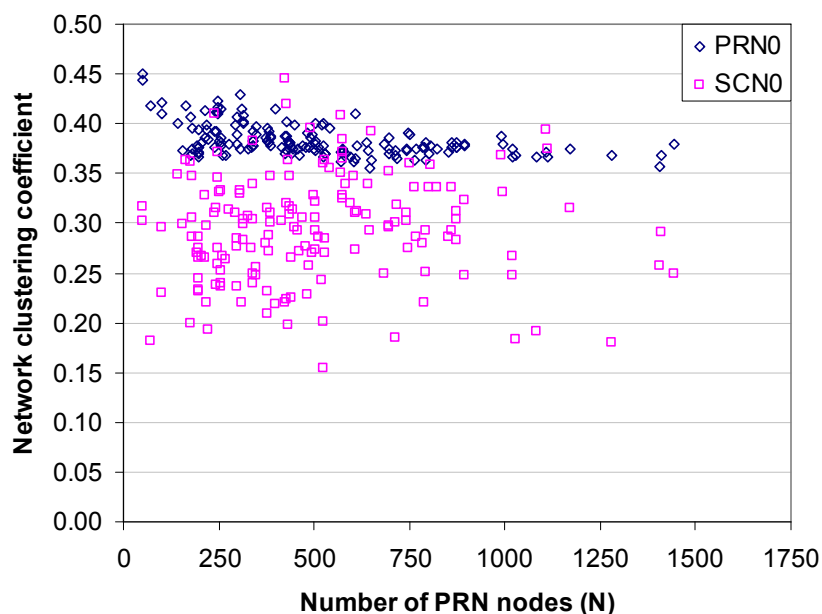


Fig. A2 Network clustering coefficients calculated with PRN0 and with SCN0 edge sets for the 166 proteins in [12]. The network clustering coefficients appear independent of N .

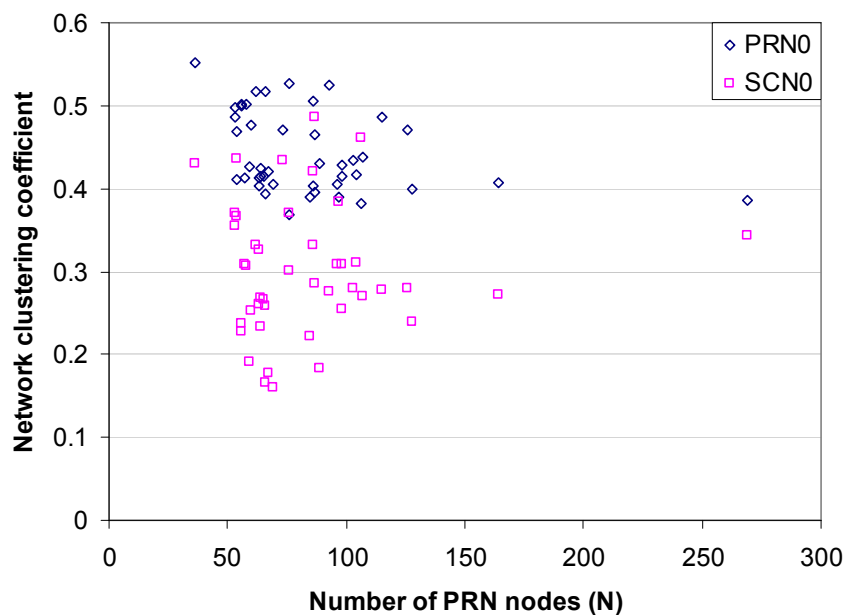


Fig. A3 Network clustering coefficients calculated with PRN0 and with SCN0 edge sets for the 44 proteins in Table A4. The network clustering coefficients appear independent of N .

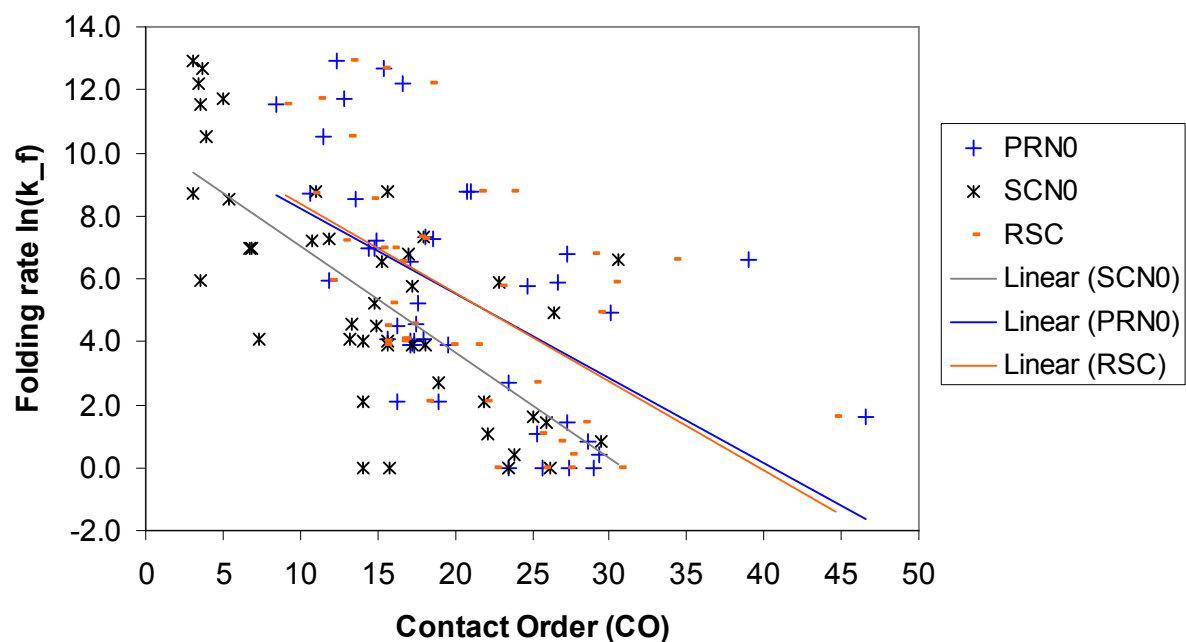


Fig. A4 Relationship between folding rate and contact order for the 44 proteins in Table A4.

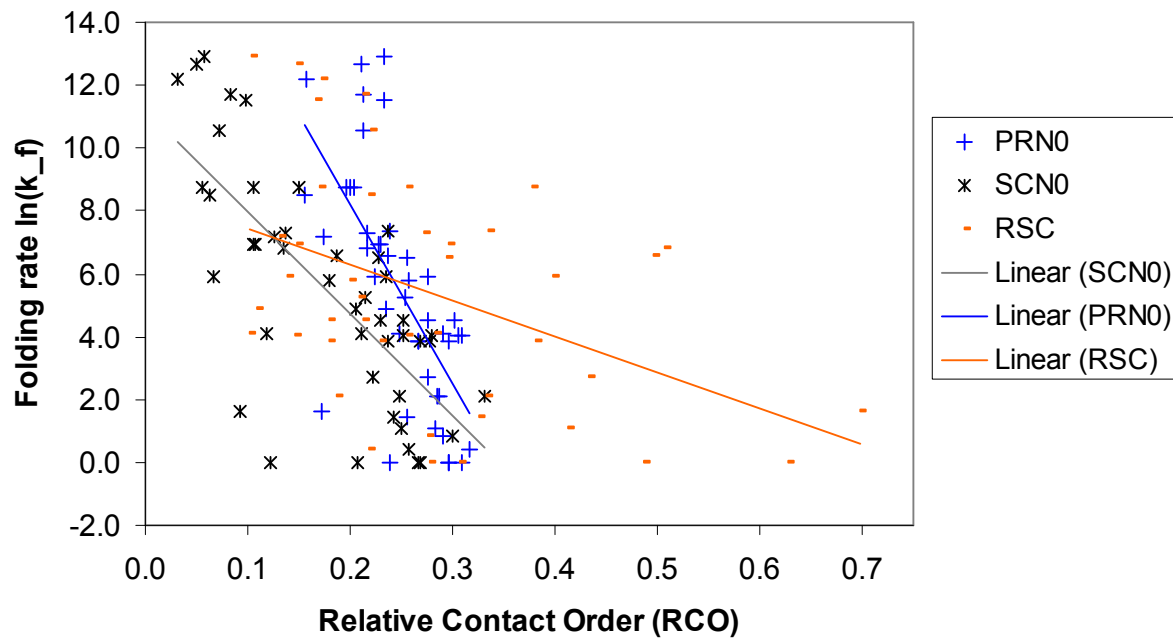


Fig. A5 Relationship between folding rate and relative contact order for the 44 proteins in Table A4.

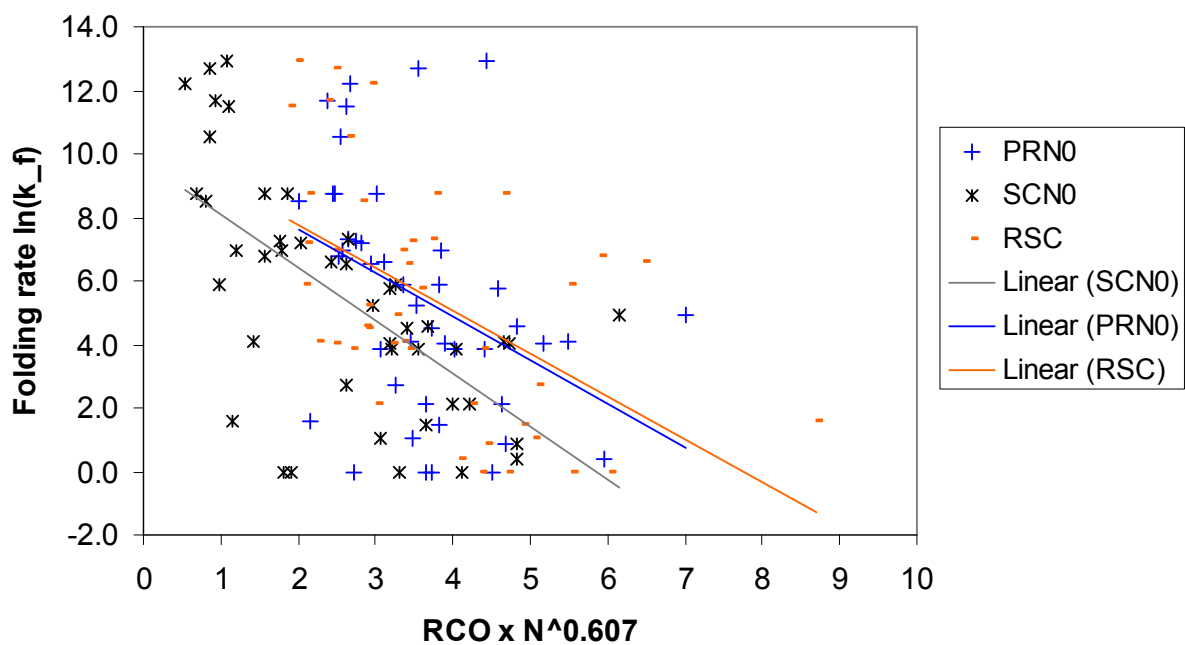


Fig. A6 Relationship between folding rate and relative contact order scaled with protein chain length [41] for the 44 proteins in Table A4.

Appendix B Supporting Material for section 3.3

Table B1 Protein folding pathways identified by C_{SCN0} and by **E** with the RBC model. Yang & Sze folding pathways [13] are provided for reference where available. 'same' denotes that the pathway is identical to the one in the previous column on the left.

PDB ID	C_{SCN0} folding pathway	E folding pathway	Yang & Sze'a folding pathway
1BDD	$(1H (3H 5H)_1)_2$	same	same
2IGD	$((1S 3S)_2 (5H (7S 9S)_1)_3)_4$	same	Not applicable.
1GB1	$((0S 2S)_2 (4H (6S 8S)_1)_3)_4$	same	$((4H (6S 8S)_1)_2 0S)_3 2S)_4$
2PTL	$((0S 2S)_1 4H)_3 (6S 8S)_2)_4$	same	$((6S 8S)_2 (0S 2S)_1)_3 4H)_4$
1MHX	$((1S 3S)_1 5H)_3 (7S 9S)_2)_4$	$((1S 3S)_2 5H)_3 (7S 9S)_1)_4$	$((7S (9S (1S 3S)_1)_2)_3 5H)_4$
1MI0	$((1S 3S)_1 (5H (7S 9S)_2)_3)_4$	same	$((7S (9S (1S 3S)_1)_2)_3 5H)_4$
2CI2	$((1S 3H)_3 ((5S 7S)_1 9S)_2)_4$	$(1S ((3H (5S 7S)_1)_2 9S)_3)_4$	$(1S ((3H (5S 7S)_1)_2 9S)_3)_4$

A folding pathway is described succinctly using a numbered parentheses format. A unique positive integer is associated with each pair of parentheses to record the fold order unambiguously. SSUs in smaller numbered parentheses combine earlier. For example, $((0S 2S)_1 4H)_3 (6S 8S)_2)_4$ describes the following sequence of fold events: (i) β -strand SSEs 0S and 2S form SSU(0S 2S), (ii) β -strand SSEs 6S and 8S form SSU(6S 8S), (iii) SSU(0S 2S) and α -helix SSE (4H) form SSU(0S 2S 4H), and (iv) SSU(6S 8S) and SSU(0S 2S 4H) form SSU(0S 2S 4H 6S 8S).

The following notes apply to Figs. B1 ... B6.

In the contact maps (adjacency matrices), shortcuts are marked by red cells, non-shortcut edges by black cells, and hydrogen bonds by green cells (in the lower triangle only).

In the search trees, C_{SCN0} and **E** folding pathways are traced by green and blue arcs respectively. Grayed out boxes are unfeasible Conformations. Dashed arcs connect (kinetically) accessible (within our RBC model) Conformations. To reduce clutter, not all accessible relations between Conformations are shown. All *entry-point* Conformations, i.e. Conformations that could be visited just prior to the native Conformation, are also included in the diagram to depict the fitness landscape around the native Conformation.

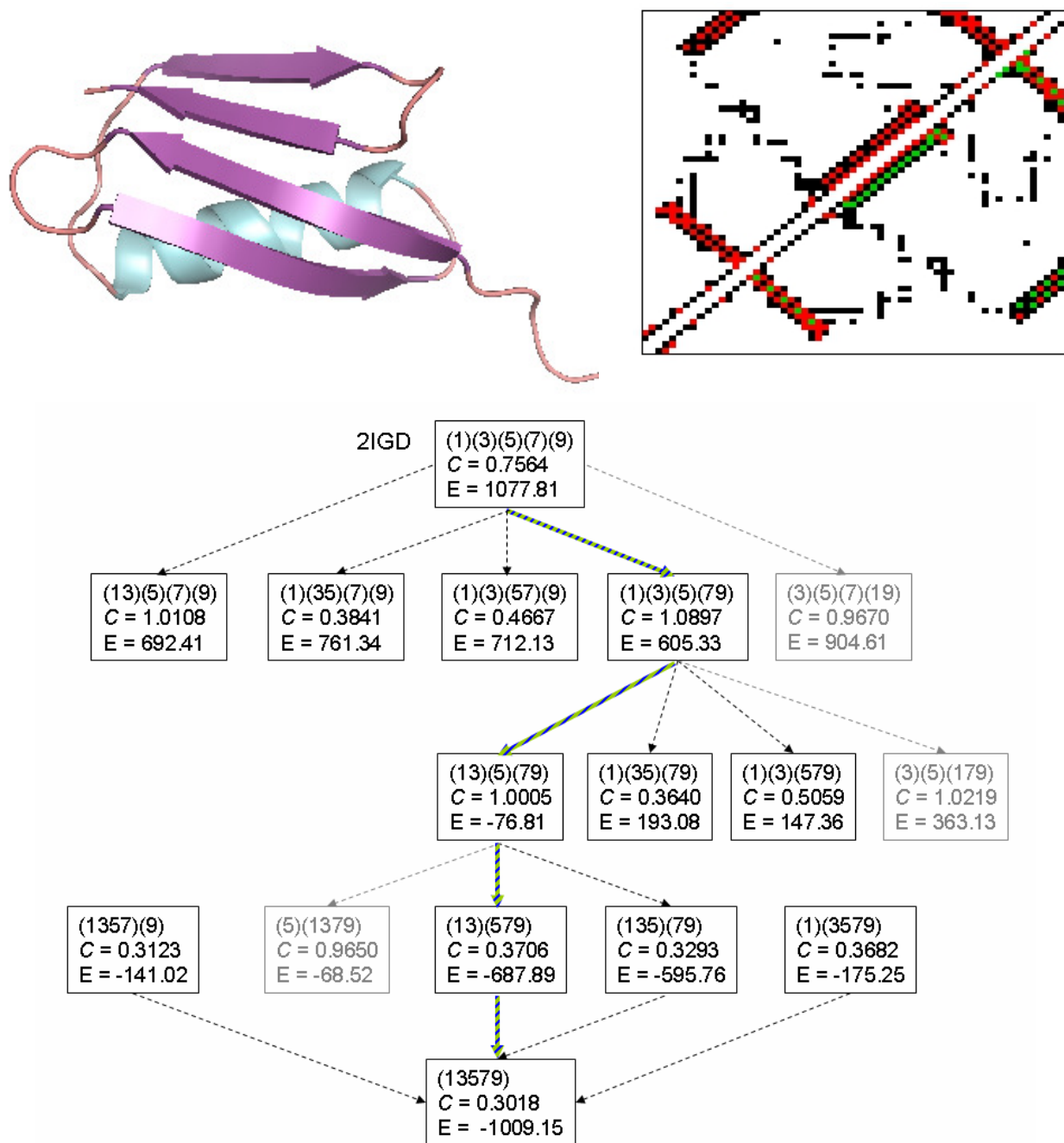


Fig. B1 Top: Cartoon of 2IGD and adjacency matrix of 2IGD's PRN. Bottom: Construction of 2IGD's C_{SCN0} (green arcs) and E (blue arcs) folding pathways. In the case of 2IGD, the native Conformation has the lowest energy and both C_{SCN0} and E folding pathways traverse the entry-point Conformation with the lowest energy.

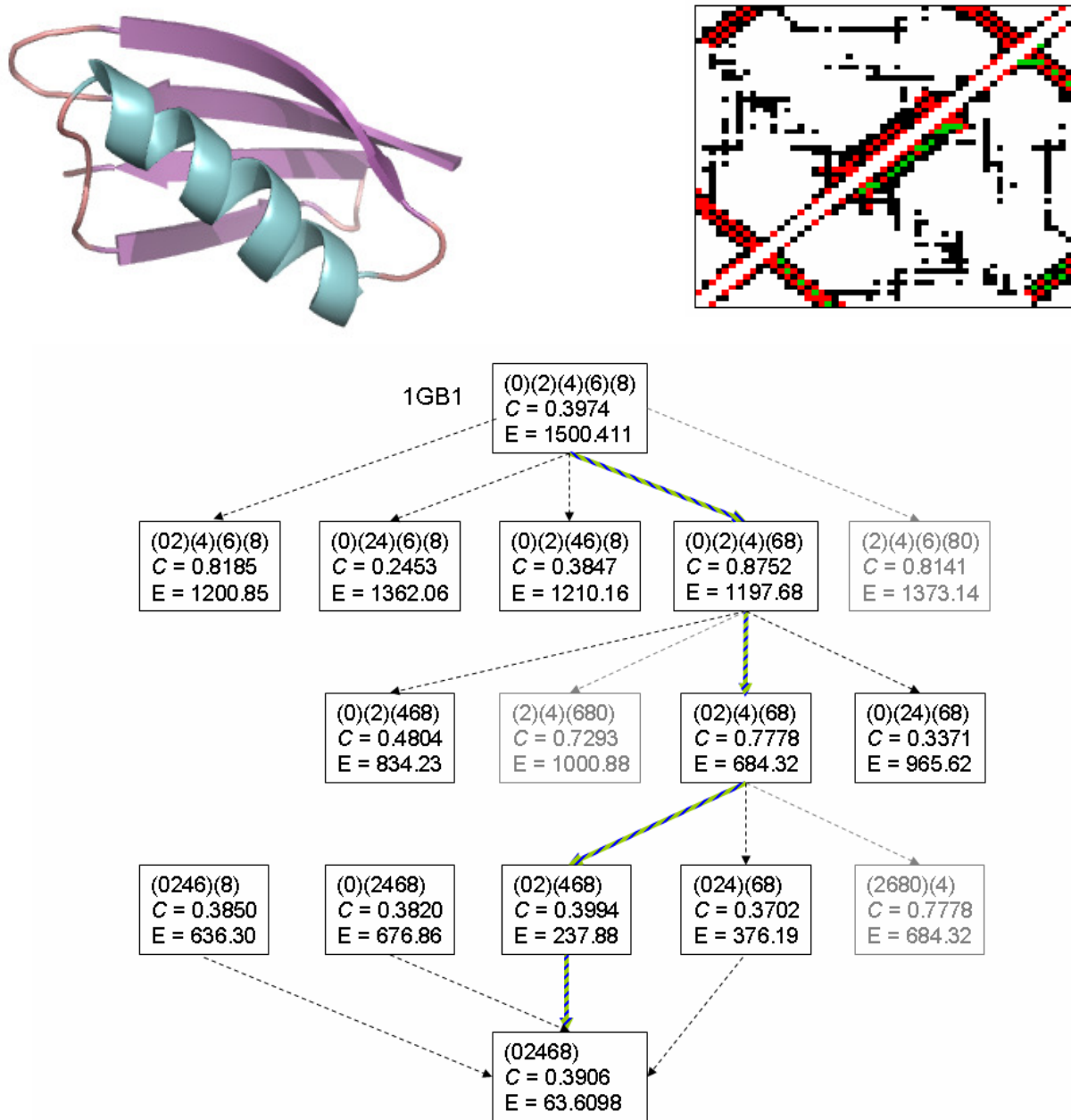


Fig. B2 Top: Cartoon of 1GB1 and adjacency matrix of 1GB1's PRN. Bottom: Construction of 1GB1's C_{SCN0} (green arcs) and E (blue arcs) folding pathways. In the case of 1GB1, the native Conformation has the lowest energy and both C_{SCN0} and E folding pathways traverse the entry-point Conformation with the lowest energy.

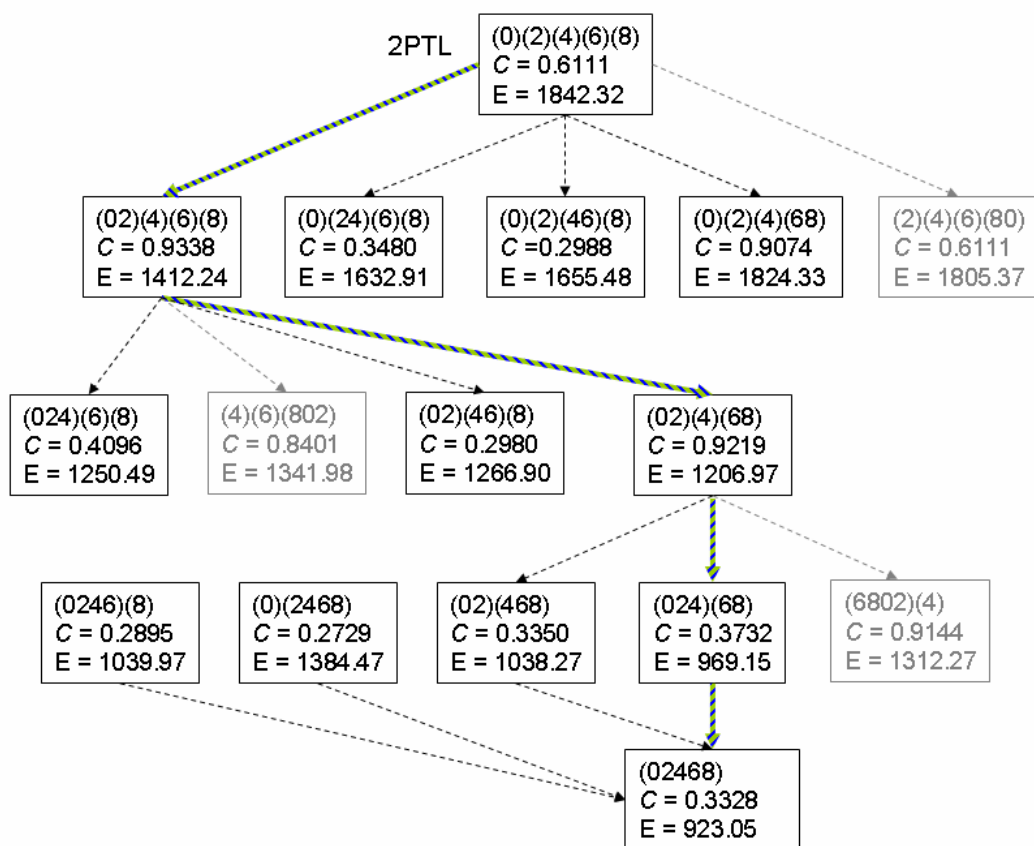
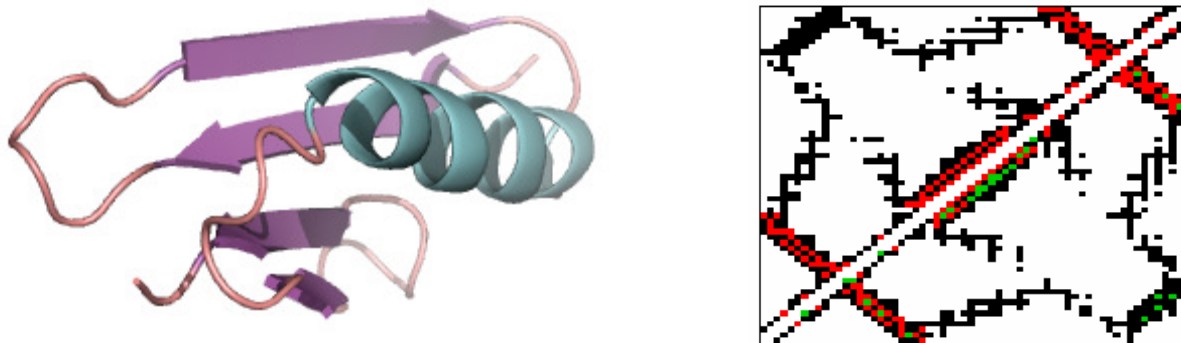


Fig. B3 Top: Cartoon of 2PTL and adjacency matrix of 2PTL's PRN. Bottom: Construction of 2PTL's C_{SCN0} (green arcs) and E (blue arcs) folding pathways. In the case of 2PTL, the native Conformation has the lowest energy, and both C_{SCN0} and E folding pathways traverse the entry-point Conformation with the lowest energy.

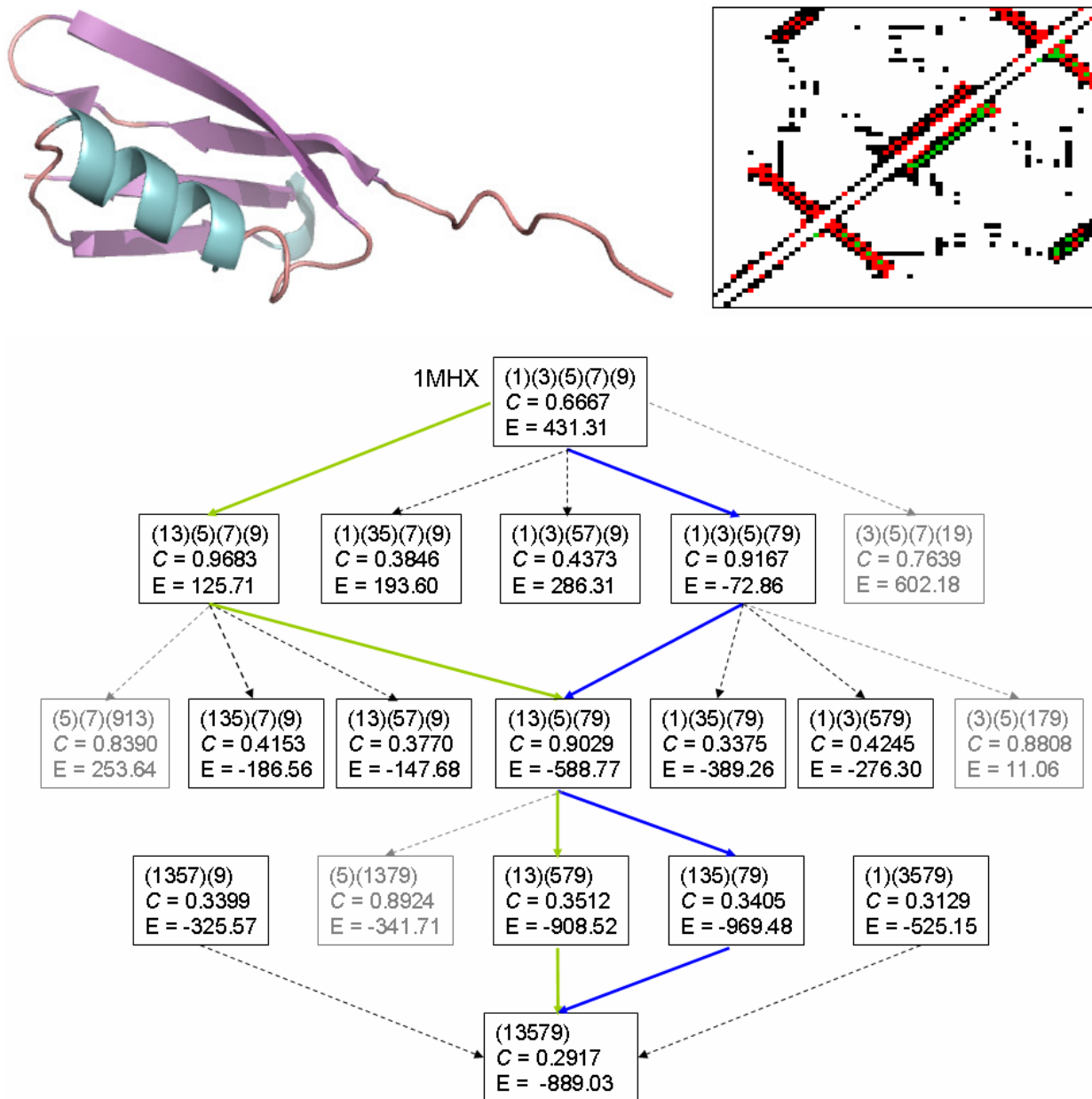


Fig. B4 Top: Cartoon of 1MHX and adjacency matrix of 1MHX's PRN. Bottom: Construction of 1MHX's C_{SCN0} (green arcs) and E (blue arcs) folding pathways. In the case of 1MHX both C_{SCN0} and E folding pathways traverse entry-point Conformations with lower energies than the native Conformation. Interestingly, the energy barrier associated with the last step on the C_{SCN0} folding pathway is smaller than that faced on the E folding pathway.

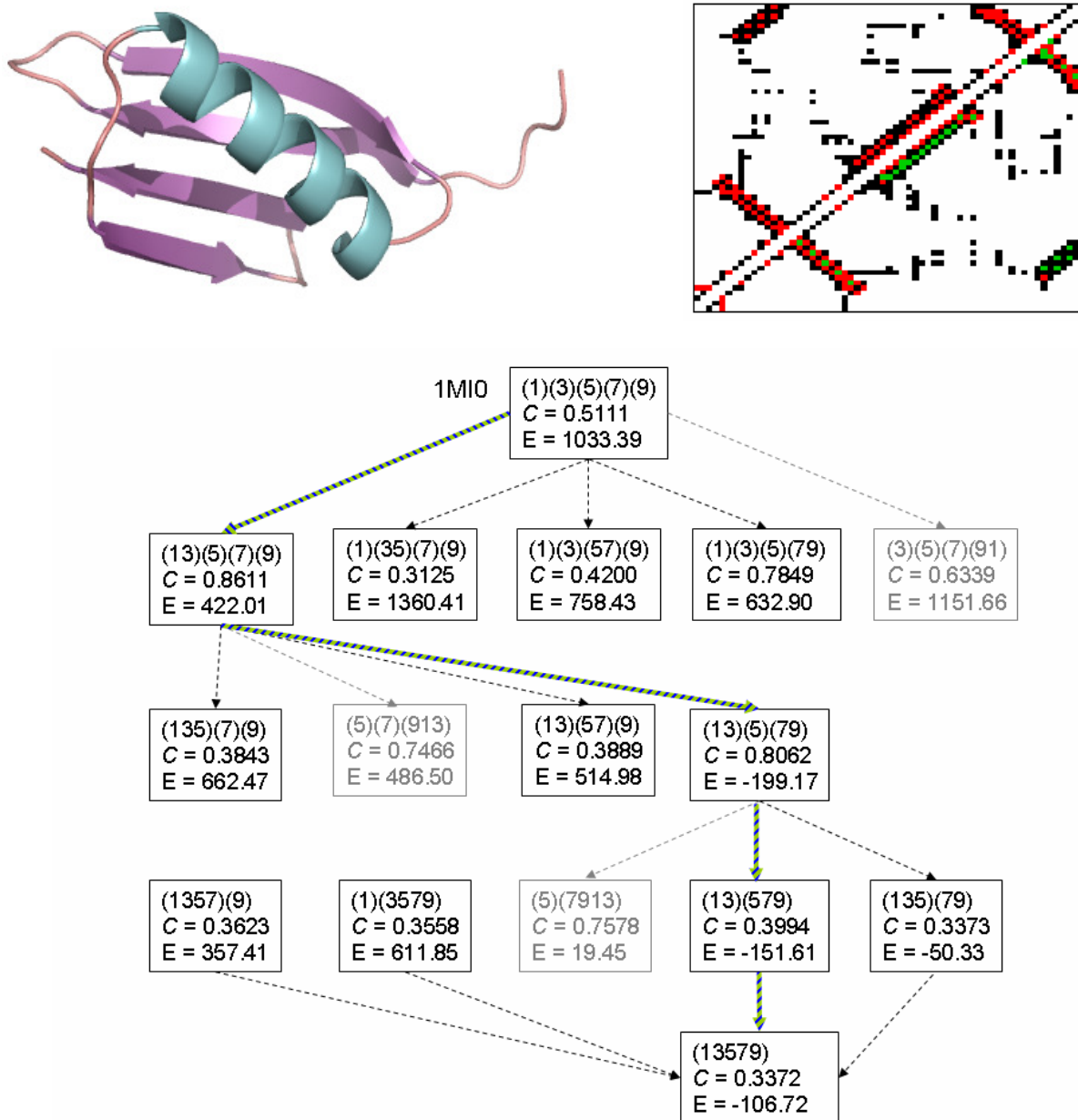


Fig. B5 Top: Cartoon of 1MI0 and adjacency matrix of 1MI0's PRN. Bottom: Construction of 1MI0's C_{SCN0} (green arcs) and E (blue arcs) folding pathways. In the case of 1MI0, both C_{SCN0} and E folding pathways traverse Conformations with lower energies than the native Conformation.

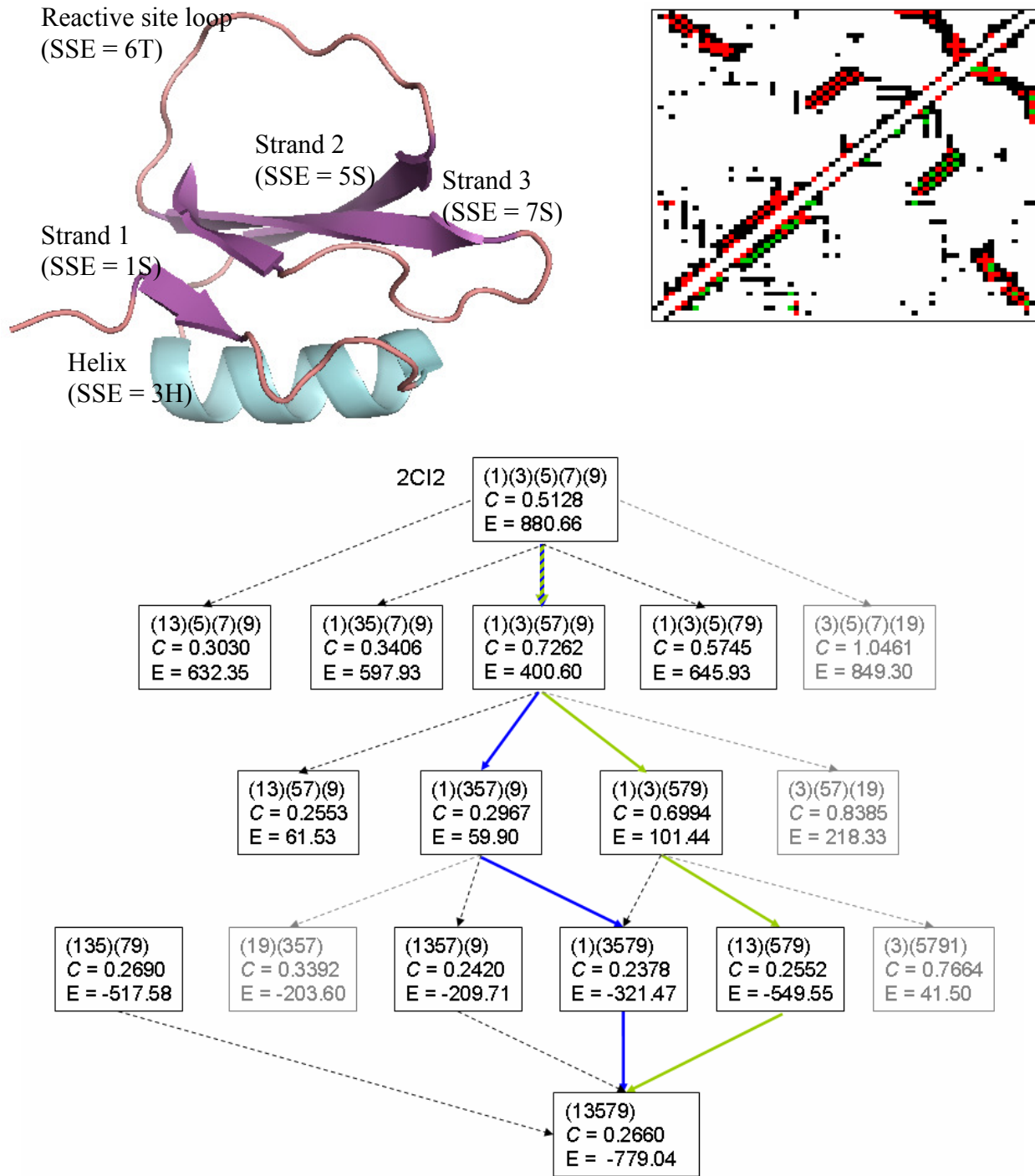


Fig. B6 Top: Cartoon of 2CI2 and adjacency matrix of 2CI2's PRN. Bottom: Construction of 2CI2's C_{SCN0} (green arcs) and E (blue arcs) folding pathways. In the case of 2CI2, the native Conformation has the lowest energy, and the C_{SCN0} folding pathway traverses the entry-point Conformation with the lowest energy.

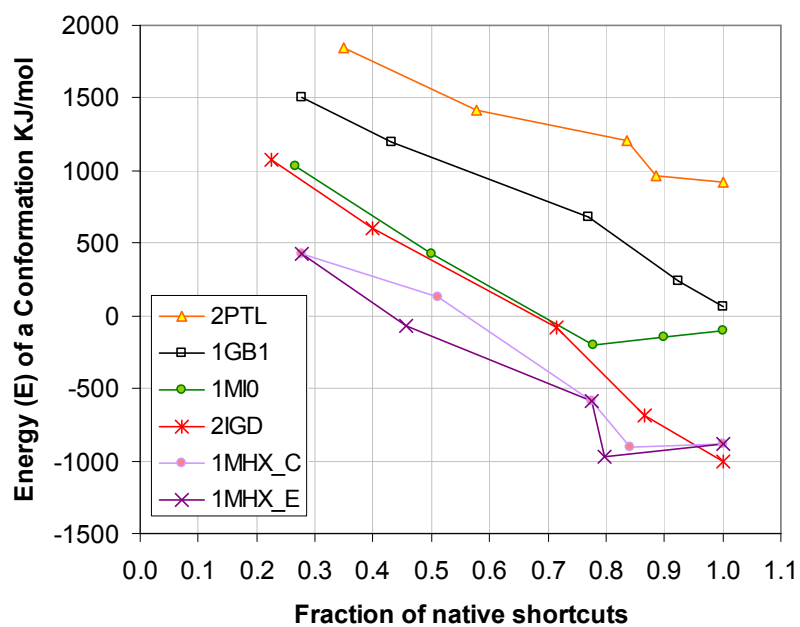
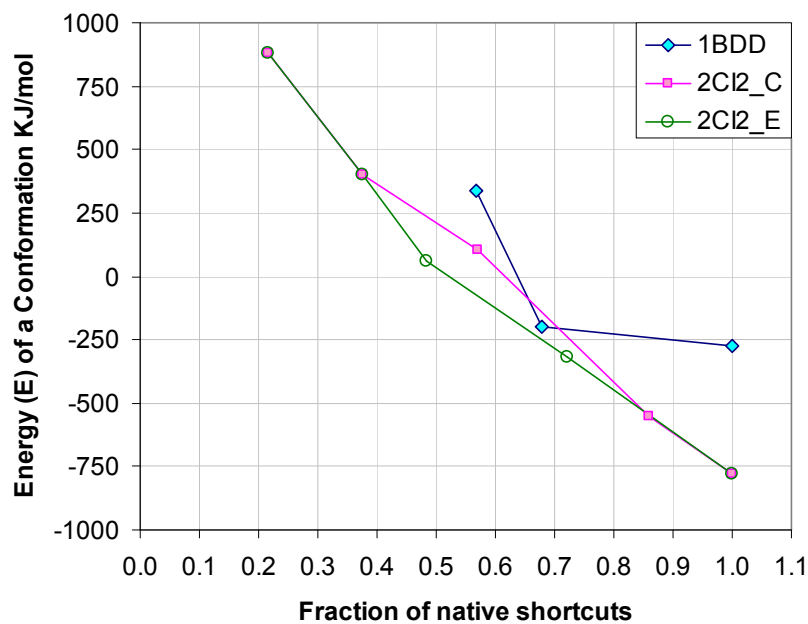


Fig. B7 Energy of Conformations on C_{SCN0} and on **E** identified folding pathways plotted against their fraction of a protein's native shortcuts. The plots for a protein are suffixed with **_C** and **_E** respectively, as is the case for both 2CI2 and 1MHX, when their C_{SCN0} and **E** folding pathways differ.

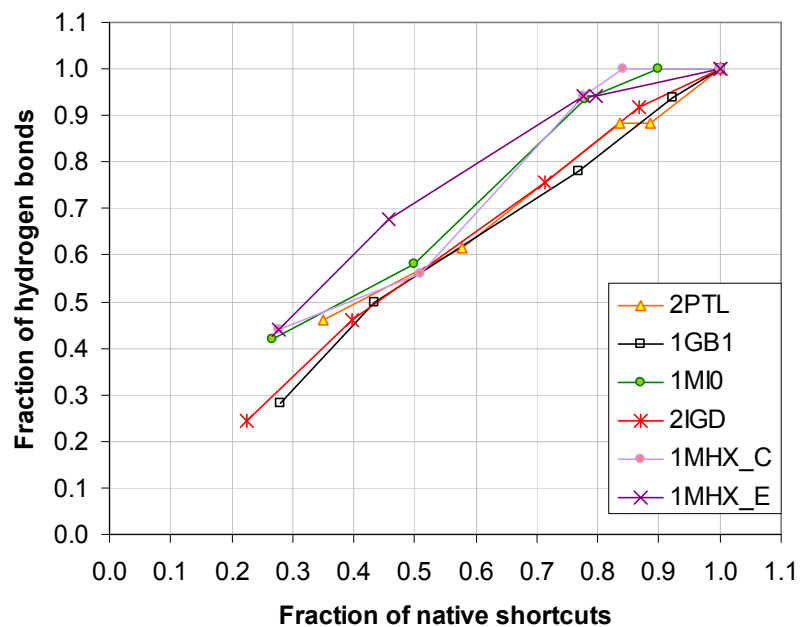
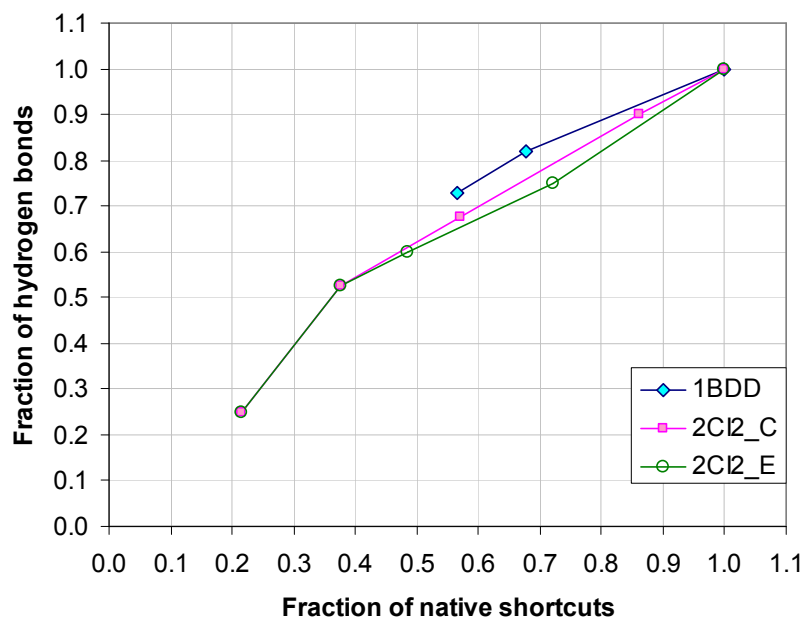


Fig. B8 Fraction of a protein's hydrogen bonds in Conformations on C_{SCN0} and on **E** identified folding pathways plotted against their fraction of a protein's native shortcuts. The plots for a protein are suffixed with **_C** and **_E** respectively, as is the case for both 2CI2 and 1MHX, when their C_{SCN0} and **E** folding pathways differ.

Appendix C

Tables C1 to C6 demonstrate the difficulty of coming up with a consistent search rule for identifying plausible folding pathways in our RBC model, using topological metrics other than C_{SCN0} .

Table C1 Fitness of 1BDD's Conformations evaluated using different metrics

Conformation	C_{SCN0}	Number of SCN0 edges	Number of PRN0 edges	C_{PRN0}	Number of hydrogen bonds
(1H)(3H)(5H)	1.2090	51	126	1.7998	32
(1H 3H)(5H)	0.5272	61	204	1.0624	37
(1H)(3H 5H)	0.8128	61	199	1.1830	36
(1H 5H)(3H)	0.7646	68	231	1.0486	35
(1H 3H 5H)	0.2534	90	437	0.4802	44

Table C2 PRN clustering score (C_{PRN0}) of feasible Conformations that are candidates for the initial fold step.

Conformation	1MHX	1MI0	Conformation	2PTL
(1S 3S)(5H)(7S)(9S)	0.925	0.945	(0S 2S)(4H)(6S)(8S)	1.009
(1S)(3S 5H)(7S)(9S)	0.352	0.464	(0S)(2S 4H)(6S)(8S)	0.510
(1S)(3S)(5H 7S)(9S)	0.357	0.434	(0S)(2S)(4H 6S)(8S)	0.430
(1S)(3S)(5H)(7S 9S)	0.957	0.983	(0S)(2S)(4H)(6S 8S)	1.049

Table C3 Number of hydrogen bonds in feasible Conformations that are candidates for the initial fold step.

Conformation	1MHX	1MI0
(1S 3S)(5H)(7S)(9S)	19	18
(1S)(3S 5H)(7S)(9S)	15	13
(1S)(3S)(5H 7S)(9S)	17	15
(1S)(3S)(5H)(7S 9S)	23	19

Table C4 RSC (shortcuts replaced by random edges) clustering score of feasible Conformations that are candidates for the initial fold step.

Conformation	2IGD	1MHX	1MI0	Conformation	1GB1	2PTL
(1S 3S)(5H)(7S)(9S)	0.175	0.042	0.038	(0S 2S)(4H)(6S)(8S)	0.303	0.111
(1S)(3S 5H)(7S)(9S)	0.110	0	0	(0S)(2S 4H)(6S)(8S)	0.167	0.067
(1S)(3S)(5H 7S)(9S)	0.035	0.095	0	(0S)(2S)(4H 6S)(8S)	0.122	0.030
(1S)(3S)(5H)(7S 9S)	0.111	0.060	0.167	(0S)(2S)(4H)(6S 8S)	0.110	0.167

Table C5 Density of shortcuts in feasible SSUs at the initial fold step.

	SSU	1GB1	2PTL	SSU	2IGD	1MHX	1MI0
N-terminal β -hairpin	(0S 2S)	0.175	0.108	(1S 3S)	0.129	0.137	0.137
	(2S 4H)	0.103	0.093	(3S 5H)	0.083	0.071	0.076
	(4H 6S)	0.109	0.090	(5H 7S)	0.105	0.087	0.090
C-terminal β -hairpin	(6S 8S)	0.190	0.203	(7S 9S)	0.181	0.198	0.220

Table C6 Density of edges in feasible SSUs at the initial fold step.

	SSU	1GB1	2PTL	SSU	2IGD	1MHX	1MI0
N-terminal β -hairpin	(0S 2S)	0.357	0.329	(1S 3S)	0.304	0.305	0.321
	(2S 4H)	0.379	0.333	(3S 5H)	0.277	0.252	0.330
	(4H 6S)	0.359	0.304	(5H 7S)	0.279	0.260	0.313
C-terminal β -hairpin	(6S 8S)	0.429	0.438	(7S 9S)	0.390	0.429	0.451

Notes on Tables C2 and C3:

- Let NS be the set of residues belonging to an SSU, and $|NS|$, the size of this set. Density of shortcuts (edges) of a SSU = $[2 \times \text{number of shortcuts(edges) with both endpoints in NS}] / [|NS| \times (|NS| - 1)]$.

Within their COMMA framework, ref. [28] proposed a metric called *communication strength* between a pair of SSEs A and B, $CS(A, B)$, to predict the order in which the helices of 1BDD would combine into the native Conformation. $CS(A, B)$ depends on the construction of communication pathways using information from a protein's native dynamics. Let (a_i, b_j) be a pair of distinct residues that are connected by p communication pathways such that a_i is a residue of SSE A, b_j is a residue of SSE B and $p > 0$. Further let S be the multiset of all (a_i, b_j) pairs traversed by the p communication pathways. $CS(A, B) = (na / nA) \times (nb / nB) \times nS$ where na is the number of unique a_i s in S , nA is the number of residues in SSE A, nb is the number of unique b_j s in S , nB is the number of residues in SSE B, and nS is the number of elements in S . SSE pairs with larger CS values, i.e. stronger communication strength, are expected to fold earlier.

Using EDS paths in place of communication pathways to calculate communication strength, we were able to arrive at the same fold order for 1BDD as ref. [28]. This method also identified the correct initial reaction points for 2PTL, 1MHX, 1MIO and 2CI2, but not for 2IGD or 1GB1 (Table C7).

Table C7 SSE communication strength using EDS paths for Initial SSUs.

Protein	Initial SSU	EDS
1BDD	(1H 3H)	9.4231
	(3H, 5H)	28.8
	(5H, 1H)	28
1GB1	(0S 2S)	32
	(2S 4H)	12.4615
	(4H 6S)	10.2
	(6S 8S)	21
	(8S 0S)	22.75
2PTL	(0S 2S)	45
	(2S 4H)	22.0444
	(4H 6S)	12.25
	(6S 8S)	38
	(8S 0S)	39
1MHX	(1S 3S)	37
	(3S 5H)	5.66667
	(5H 7S)	1.05
	(7S 9S)	18
	(9S 1S)	21.3333
1MIO	(1S 3S)	33
	(3S 5H)	16.3333
	(5H 7S)	5.54667
	(7S 9S)	18
	(9S 1S)	20.125
2CI2	(1S 3H)	2.87179
	(3H 5S)	2.30769
	(5S 7S)	32
	(7S 9S)	12
	(9S 1S)	10
2IGD	(1S 3S)	28
	(3S 5H)	4.7473
	(5H 7S)	2.7692
	(7S 9S)	19
	(9S 1S)	21

Table C8 DeepView Energy of the two β -hairpins.

	SSU	1GB1	2PTL	SSU	2IGD	1MHX	1MIO
N-terminal β -hairpin	(0S 2S)	370.95	361.18	(1S 3S)	175.63	-7.80	72.88
C-terminal β -hairpin	(6S 8S)	482.94	667.01	(7S 9S)	155.41	50.54	278.52

Appendix D Supporting material for section 3.4

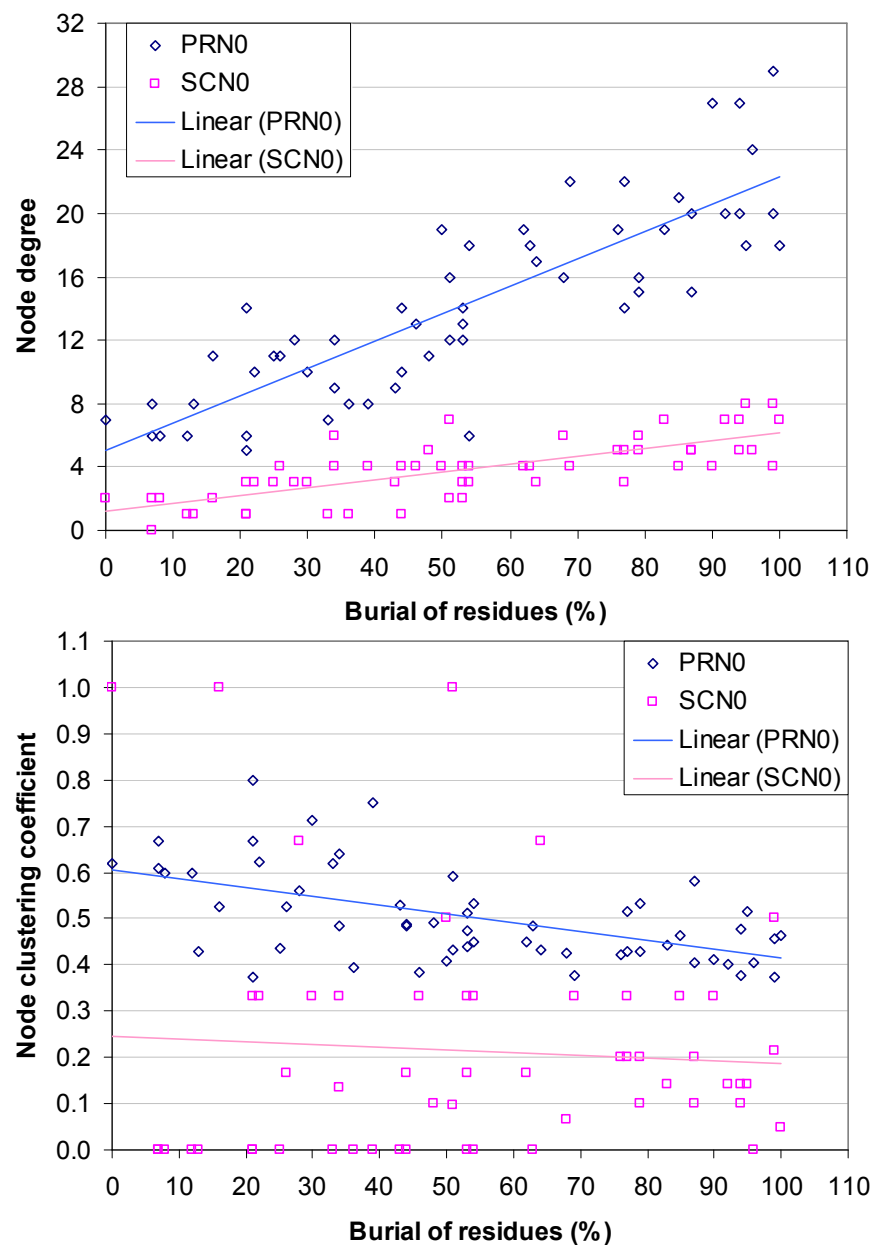


Fig. D1 Top: Pearson's correlation coefficient for PRN0 node degree and Burial of residues is 0.8448 (p-val=2.22E-16), and for SCN0 node degree and Burial of residues is 0.7442 (p-val=4.92E-11). Bottom: Pearson's correlation coefficient for PRN0 node clustering and Burial of residues is -0.5500 (p-val=1.13E-05), and for SCN0 node clustering and Burial of residues is -0.0667 (p-val=0.6249).

In Figs. D2 to D6, nodes are sorted by PRN0 node degree in descending order and by PRN0 node clustering in ascending order.

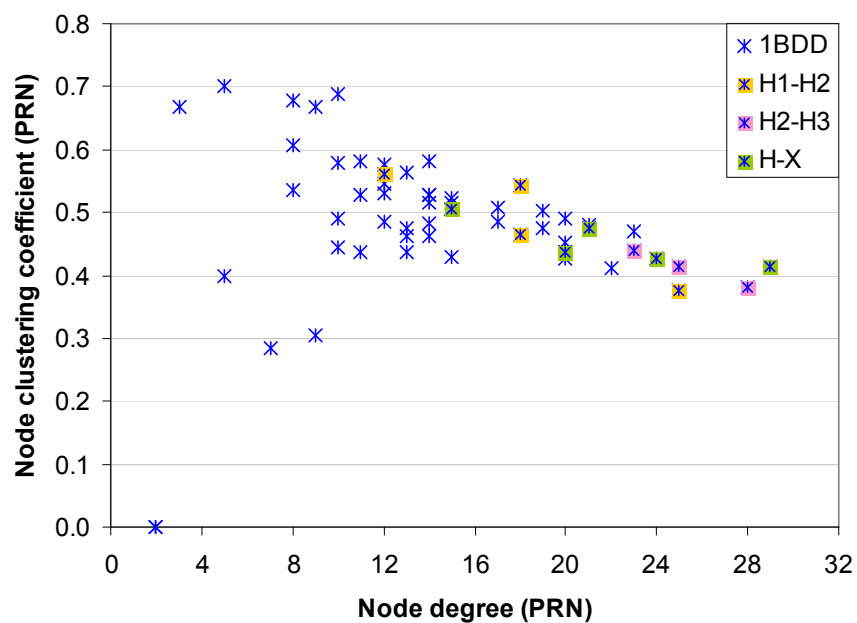


Fig. D2 Key folding residues for 1BDD are highlighted in pink, orange and green. H-X sites which are not also H1-H2 or H2-H3 sites are highlighted.

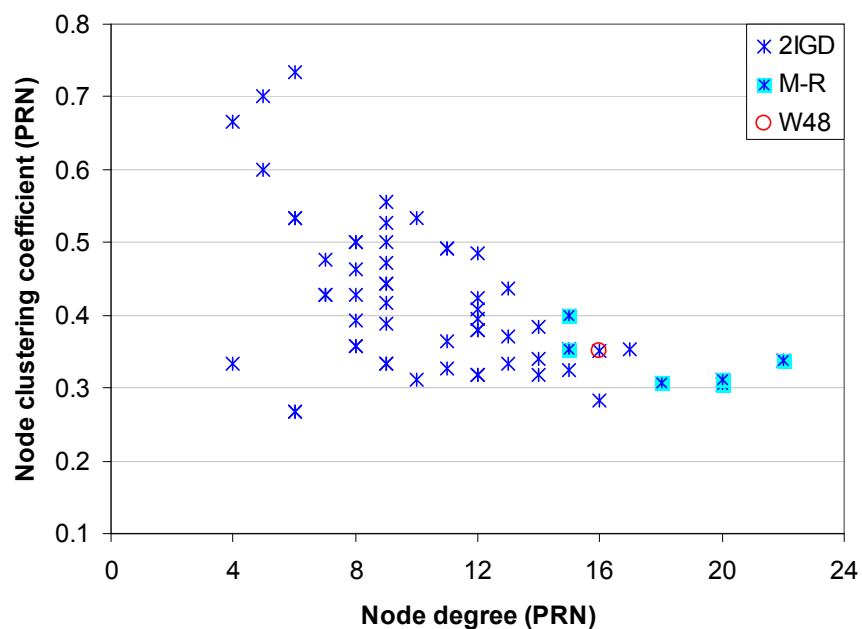


Fig. D3 Key folding residues for 2IGD are highlighted in blue.

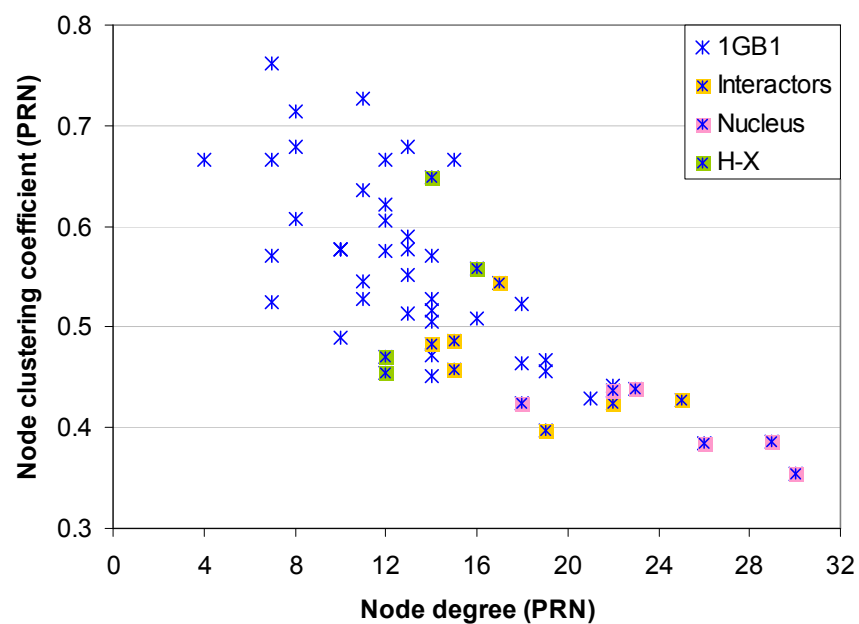


Fig. D4 Key folding residues for 1GB1 are highlighted in pink, orange and green. Interactor residues are those that partner with a Nucleus residue in Table 1 of ref. [24]. H-X sites which do not also fall in the other two categories are highlighted.

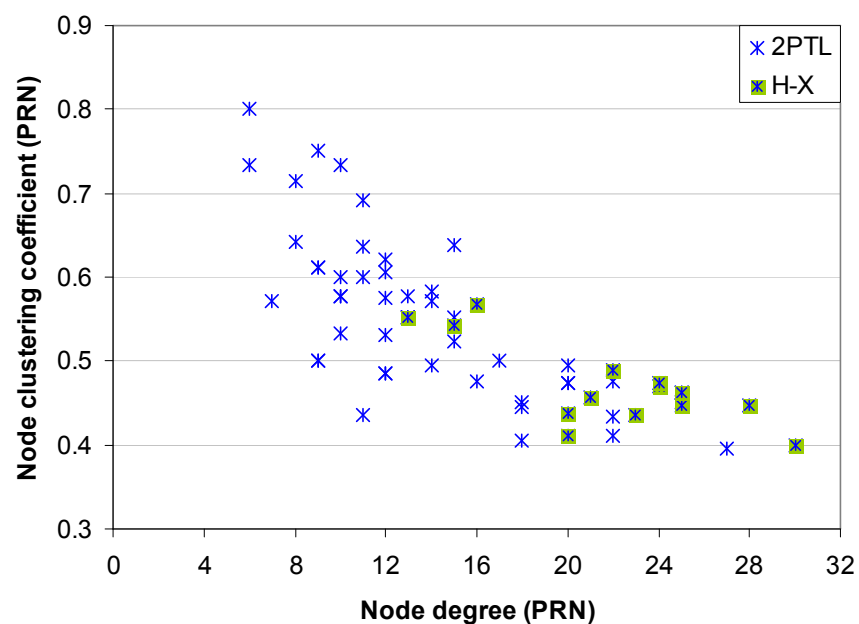


Fig. D5 Key folding residues for 2PTL are highlighted in green.

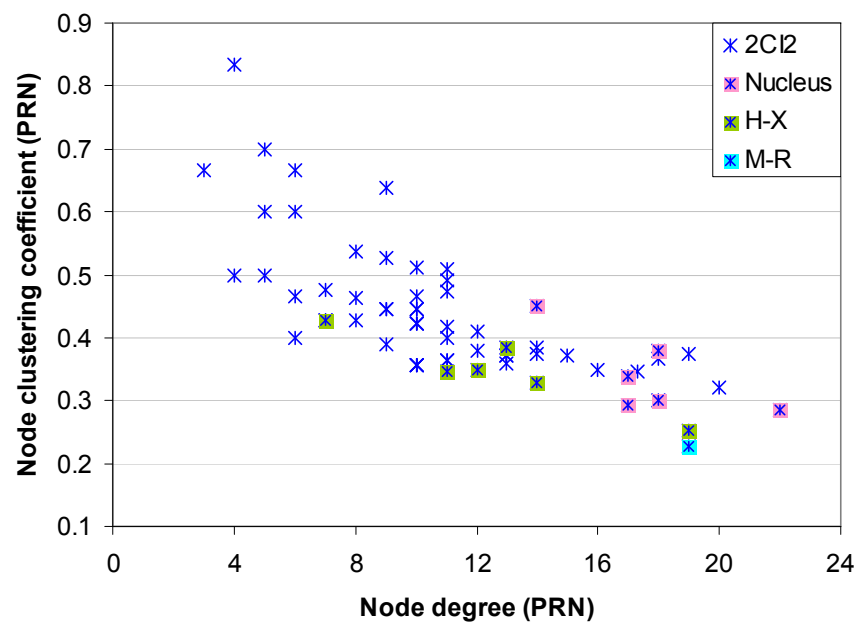


Fig. D6 Key folding residues for 2CI2 are highlighted in pink, green and blue. H-X sites which are not also nucleation sites are highlighted. M-R sites which are not also nucleation or H-X sites are highlighted.